46
11/6/95 95 (2)

SANDIA REPORT

SAND95–2141 • UC–404
Unlimited Release
Printed October 1995

Fundamental Science of Nanometer-Size Clusters

J. P. Wilcoxon, P. P. Newcomer, G. A. Samara,
E. L. Venturini, R. L. Williamson

Prepared by
Sandia National Laboratories
Albuquerque, New Mexico 87185 and Livermore, California 94550
for the United States Department of Energy
under Contract DE-AC04-94AL85000

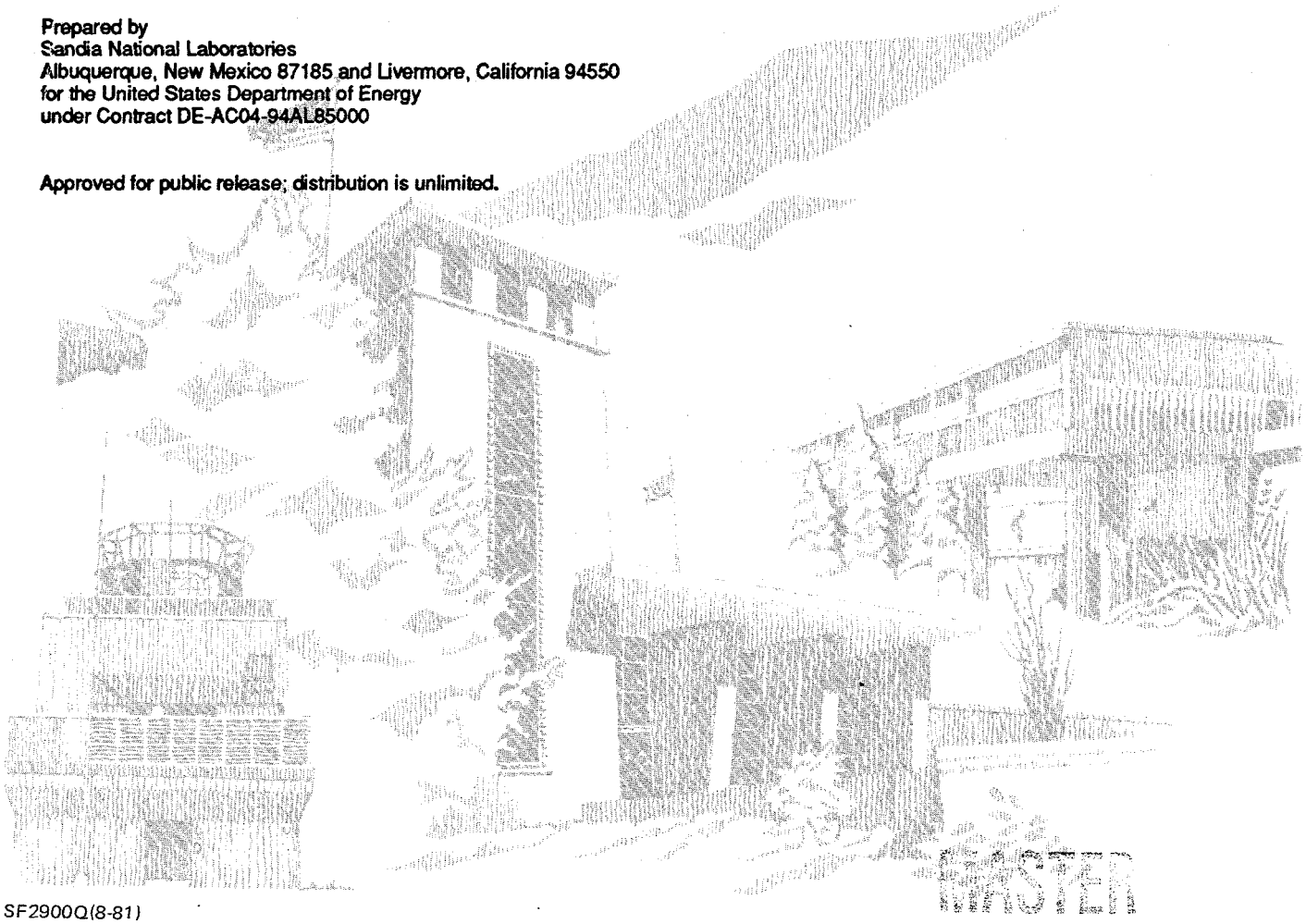

SAND95-2141
Unlimited Release
Printed October 1995

Distribution
Category UC-404

FUNDAMENTAL SCIENCE OF NANOMETER-SIZE CLUSTERS

J. P. Wilcoxon, P. P. Newcomer, G. A. Samara
Nanostructures & Advanced Materials Chemistry Department
E. L. Venturini
Advanced Materials Physics & Devices Department
R. L. Williamson
Liquid Metal Processing Department
Sandia National Laboratories
Albuquerque, NM 87185

Abstract

This research has produced a variety of monodisperse, nanometer-size clusters (nanoclusters for short), characterized their size and crystal structure and developed a scientific understanding of the size dependence of their physical properties. Of specific interest were the influence of quantum electronic confinement on the optical properties, magnetic properties, and dielectric properties. These properties were chosen both for their potential practical impact on various applications identified in the National Critical Technologies list (e.g., catalysis, information storage, sensors, environmental remediation, ...) as well as for their importance to the fundamental science of clusters. An Executive Summary provides a description of the major highlights.

Table of Contents

Executive Summary

The overall objective of this Laboratory-Directed Research and Development (LDRD) program was to capitalize on our recently-developed inverse micellar synthesis approach to produce a variety of monodisperse, nanometer-size clusters (nanoclusters for short), characterize their size and crystal structure and develop a scientific understanding of the size dependence of their physical properties. Of specific interest is the influence of quantum electronic confinement on the optical properties, magnetic properties, and dielectric properties. These properties were chosen both for their potential practical impact on various applications identified in the National Critical Technologies list (e.g., catalysis, information storage, sensors, environmental remediation, ...) as well as for their importance to the fundamental science of clusters. This report will show that we have produced some unique materials and have made considerable progress towards the stated ends.

In our approach, nanoclusters are grown inside inverse micellar cages in non-aqueous solvents. Inverse micelles are formed when surfactant molecules are dispersed in a non-polar (e.g., octane, oil) continuous medium. In such a medium, the hydrophilic ends of the surfactant molecules avoid the oil and form cages whose sizes typically range from 1 to 10 nanometers depending on the choice of surfactant and solvent. The polar interiors of these cages are capable of dissolving salts (without the addition of a polar solvent -- a unique feature of the Sandia process) and serve as the nanoscale reactors in which chemical reactions take place.

Highlights of the work are as follows:

- Several semiconductors nanoclusters including MoS_2, WSe_2, CdS and TiO_2 were synthesized and studied with emphasis on MoS_2 as a model system. The dependence of its optical properties on cluster size is qualiitatively representative

of the other semiconductor nanoclusters, but its layered crystal structure and high potential for applications in catalysis and photocatalysis made it a unique and challenging choice. Key results include the observation and interpretation in terms of the electronic structure of: (1) heretofore unseen and well-defined features in the absorption spectra reflecting the underlying physics as well as the high quality and monodispersity of our clusters; (2) large blue shifts in the absorption spectrum with decreasing cluster size resulting from electronic quantum confinement and affording great tailorability of the bandgap; and (3) a beautiful demonstration of the crossover from band-like (solid) to molecule-like spectra as the size of the cluster becomes smaller than that of the Bohr radius of the exciton (r_B = 2.0 nm) in the bulk.

- Iron (Fe), nickel (Ni) and cobalt (Co) nanoclusters were grown, but Fe (α, or bcc phase) was the model system studied in most detail. The saturation magnetization, remnant magnetic moment and superparamagnetic blocking temperature are strong functions of cluster size and differ considerably from literature results which are plagued by the presence of a surface oxide layer on the Fe cluster core and poor control over cluster size. Our results appear to be the only results on pure α-Fe clusters.

- We demonstrated for the first time the ability to reproducibly control the crystal structure of a nanocluster by the choice of surfactant and solvent. We grew both α-Fe and γ (fcc structure)-Fe nanoclusters at room temperature. In bulk form α-Fe is the normal equilibrium phase which transforms to the high temperature γ-Fe phase at 961 °K. γ-Fe has remarkably different magnetic properties from those of α-Fe.

- Studies of the dielectric properties of gold (Au) and palladium (Pd) nanoclusters suggest significant enhancements in the electronic polarizabilities of these materials due to quantum confinement; however, this highly significant result (from both theoretical and experimental considerations) must be considered tentative because of the presence of some residual ionic species in the samples studied. The real part of the dielectric constant (ϵ') deduced from our measurements is negative for both clusters, as is expected for metals. We do not see evidence of the puzzling large positive ϵ''s recently reported for larger ($\geq$50 nm) metallic clusters.

- We have demonstrated relatively large blue shifts in the plasmon resonances of Au and silver (Ag) nanoclusters with decreasing cluster size below ~ 10 nm. The shifts are larger than what is predicted by current theory. We have also succeeded in growing composite nanoclusters consisting of a Au core and Ag capping layer, or vice versa, and demonstrating that the capping layer has a strong influence on the optical properties.

- By growing a wide variety of metal and semiconductor nanoclusters, we have significantly improved the reproducibility and size control of the inverse micellar synthesis process.

- To separate the nanoclusters from residual species and reaction byproduct species, we have established a new high pressure liquid chromatography capability with on-line optical diagnostics. This separation/purification capability, which has allowed us to observe previously unobserved features in the optical properties of many nanoclusters, is unique to Sandia and represents a highly significant advance in the field of nanoclusters.

Finally, in this LDRD-funded work we have produced some of the highest quality nanoclusters available as well as new nanoclusters and developed a considerable understanding of the dependences of their optical, magnetic and dielectric properties on cluster size. The results have pointed out the richness of the science in this field which has great technological promise. We have just barely scratched the surface; much of the scientific and technological excitement lies ahead.

I. Introduction

Nanometer-size clusters (or nanoclusters) offer exciting opportunities in materials science, a point recently emphasized by the DOE Council on Materials Science in a Panel Report.[1] These opportunities stem from the strong size dependence of the optical, electronic, and magnetic properties of nanoclusters, which are due to spatial confinement of the electrons, the large fraction of surface atoms, and/or differences in crystal structure from the bulk material. Progress in these areas, however, has awaited the ability to produce significant yields of monodisperse clusters that are surface-stabilized against aggregation.

As part of an engineering science project on catalysis,[2] we developed a unique synthesis process, based on using inverse micelles as reaction vessels, that meets these requirements for clusters down to ~ 10-15 Å in size composed of a wide variety of materials. This process provided the basis for this Laboratory-Directed Research and Development (LDRD) program.

The overall objective of this LDRD program was to capitalize on our inverse micellar synthesis approach to produce a variety of monodisperse, nanoclusters, characterize their size and crystal structure and develop a scientific understanding of the size dependence of their physical properties. Of specific interest are the size dependence of optical properties, magnetic properties, dielectric properties and superconductivity. These properties were chosen both for their potential practical impact on various applications identified in the National Critical Technologies list as well as for their importance to the fundamental science of clusters. This report will show that we have produced some unique materials and have made considerable progress towards the stated ends. During the oral presentation of this proposal prior to its funding, members of the Technical Advisory Team (TAT) expressed concern that we were proposing to do too many things for the proposed level of funding. In view of this concern, we agreed to de-emphasize the study of superconductivity of clusters unless time permitted us to do so during the second year. As it turned out, we were not able to study this interesting area with the exception of demonstrating that we can synthesize nano-size niobium nanoclusters. We hope to study their superconducting properties in future work.

The report is organized as follows. In Sec. II we review briefly the synthesis and processing of nanoclusters in inverse micelles. In this process the clusters are produced

in solution in a nonpolar (oil) medium which generally contains excess surfactant, residual salts and reaction byproducts. In the latter phases of this program it became clear that for some of our studies it was necessary to separate the clusters from the residual and byproduct species. Toward this end we developed a new high pressure liquid chromatography capability with on-line optical diagnostics. This capability, which was recently implemented and is discussed in some detail in Sec. II, has resulted in heretofore unseen features in the optical spectra of several clusters. We believe that this capability is unique to Sandia and represents a highly significant advance in the field of nanoclusters.

Section III deals with the optical properties of semiconductor nanoclusters. We synthesized and studied several clusters (some for the first time) including MoS_2, WS_2, CdS and TiO_2. In Sec. III we concentrate on MoS_2 as a model system. The dependence of its optical properties on cluster size is qualitatively representative of other semiconductors, but its layered crystal structure and high potential for applications in catalysis and photocatalysis made it a unique and challenging choice.

Section IV covers magnetic nanoclusters. We have grown iron (Fe), nickel (Ni) and cobalt (Co) clusters, but Fe was our model system and was studied in some detail. In this work we demonstrated for the first time the ability to control not only size but the crystal structure, synthesizing both α-(bcc)- and γ–(fcc)-phase Fe clusters. α-Fe clusters prepared by other techniques have been studied by other workers, but such clusters invariably consist of an oxide layer (of generally unknown thickness and composition) and an Fe core. Our clusters represent the first oxide-free Fe nanoclusters, and, as will be shown, their magnetic properties differ significantly from those in the literature.

The dielectric properties of metallic nanoclusters are discussed in Sec. V. Emphasis is on palladium (Pd) and gold (Au) clusters which were studied in both liquid and polymeric matrices. The results suggest enhancement in the electronic polarizability due to quantum confinement, but this highly significant result (from both experimental and theoretical considerations) must be considered tentative at this time because of the presence of some residual ionic species in the samples studied. In future studies we shall repeat the measurements on chromatographically-purified samples to confirm the results.

Section VI deals with the optical properties of metallic nanoclusters. We have investigated Au, silver (Ag), Fe and Pd clusters. Some results on Au and Ag will be

presented to illustrate the dependence of the plasmon resonance on cluster size. A unique feature of our work is the synthesis of composite metal clusters and the study of their optical properties. We illustrate this aspect of the work by results on clusters consisting of Au cores and Ag shells or vice versa.

Finally, Sec. VII provides some concluding remarks on future directions of this work. In many respects we have just barely scratched the surface. The work accomplished under this LDRD program has been exploratory in nature. It has produced some of the highest quality clusters available as well as new clusters, and it has pointed out the richness of the science in this field of science.

II. Synthesis and Processing of Nanosize Clusters In Inverse Micelles

A. Cluster Synthesis

We have developed a new method for the formation of nanosize metal clusters in organic media and have recently obtained a patent on this technique.[3] Our intent in our earlier work was to employ these clusters as unsupported catalysts for *in situ* chemical reactions such as coal liquefaction, removal of sulfur from coal, and for other catalytic applications.[4,5] In the present work we have improved the process and extended it to the formation of a variety of elemental and compound clusters.

Metal clusters are prepared in the microheterogeneous environment of an inverse micelle solution.[5] Inverse micelles are defined as surfactant aggregate clusters (droplets) surrounded by an oil-like continuous environment. Polar molecules such as water are often dissolved in the interior of these micelles forming solutions called microemulsions. These solutions are clear because the droplet sizes are very small, typically 2-20 nm, so they do not scatter light strongly. In our method, we use the polar interiors of the micelles to directly solubilize metal salts (e.g. $PdCl_2$). Our process is shown schematically in figure 1.

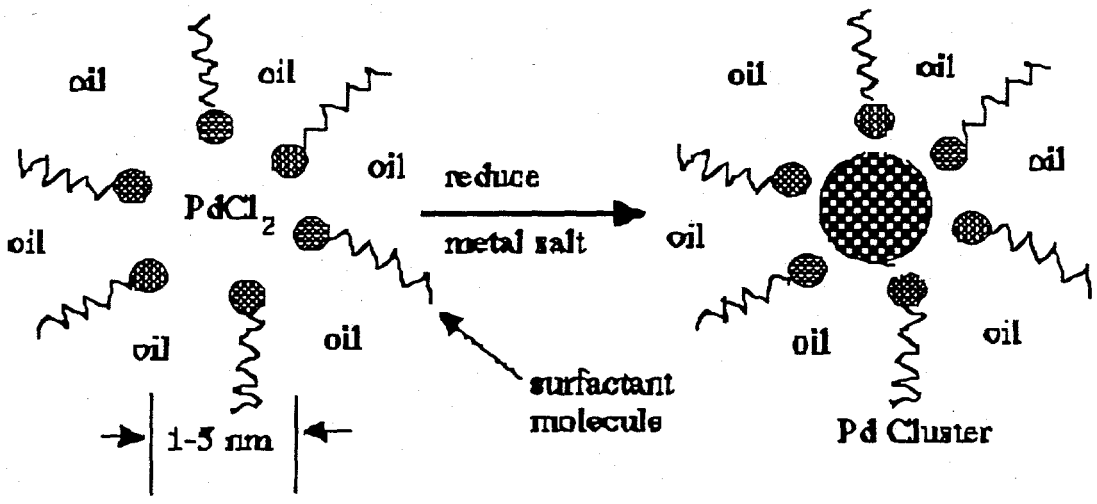

Figure 1. Scheme for formation of a palladium metal cluster in an inverse micelle. Typical interior micelle size of 1-5 nm is indicated. The squiggly hydrocarbon tail groups form an interface with the continuous oil medium.

For most metals no water is used in the solubilization process. The resulting solution is colored but transparent, demonstrating the microscopic size of the metal salt encapsulated droplets. These precursor solutions are truly remarkable since they are homogeneous, stable, transparent dispersions of charged metal ions in oil! Several methods of reduction may then be used to reduce the metal cation to the zero valence state. Controlled nucleation and growth in the interior of the micelle droplet occurs which typically results in a small metal cluster (typical size 1-20 nm). The micelle environment allows both size control and stabilization of the final clusters against unwanted aggregation. The surfactant, being a surface active organic molecule, adheres to the metal cluster preventing aggregation, yet, might still allow access to the surface for catalytic reactions.

An inert oil environment also enables unique reduction chemistry. For example, sodium or lithium metal dispersions may be used for the reduction of the metal ions. We have applied this reduction method for metal ions which cannot be easily reduced by conventional chemical agents such as Si(IV). Such strong agents ensure complete reduction to the zero valance state.

Clusters of compounds such as metal sulfides and oxides can be formed by mixing two precursor micelle solutions, e.g. $Fe(ClO)_2$ and Na_2S, which would ordinarily form a bulk precipitate of FeS_2. We also used H_2S gas as a sulfiding agent. Metal oxides (e.g. TiO2) may be formed by forced hydrolysis of a metal ion (e.g. $TiCl_4$) using a base such as NaOH.

Heterogeneous nucleation and growth of one material on another nanosize material has also been demonstrated as part of this program. In this process a seed population of small clusters (e.g. Fe) is first prepared as outlined above and subsequently coated with another metal (e.g. Ir). Potentially, this could allow, for example, disposable catalysts to be developed, (such as Pt or Ir on Fe or Ni), which is a major economic requirement for any successful coal liquefaction process.

It is interesting to note that in the absence of special intermicellar interactions (i.e. phase boundaries), the final cluster size closely reflects that of the precursor micelle. This is because only clusters smaller than the micelle interior diameter can be solubilized in the hydrophilic micelle interior. In general, our micellar synthesis method allows a much greater variety of sizes, types of materials, and concentration ranges than classical methods for colloid formation in homogeneous solution.

B. Cluster Separation and Purification

One of the characteristics of our inverse micellar synthesis approach is the presence of reaction byproducts such as inorganic ion pairs and excess surfactant in the final solution containing the clusters. While we were able to study many properties of the resulting clusters in the presence of these various species, it became clear in the latter phases of this work that for some studies it is necessary to separate them from the clusters.

In a previous SAND report[2], we described simple methods based upon micelle phase separation in which ionic byproducts could be removed from nonionic ones, including the clusters. This is illustrated schematically in figure 2. Using GC/MS of the two coexisting phases shown in this figure, we determined that only 80% of the surfactant could be removed by this process so we undertook as part of the present work the development of new methods of high pressure liquid chromatography to separate the desired products (clusters) from reactants (surfactants, oils, and inorganic salts). We believe that this development is highly significant for the future study and utilization of clusters grown by inverse micellar and other solution methods.

Because inorganic clusters with sizes small enough to penetrate the typical pore sizes of commercially available chromatography columns were not available prior to our work, virtually nothing is known about the interactions between such inorganic materials and typical organic column materials. Conventionally, two types of retention mechanisms take place in typical chromatographic separations. In the first, called size-exclusion chromatography, molecules are sorted by their ability to penetrate into the pores of the column. Small molecules spend proportionally more time in these pores and thus elute from the column later than large ones. The most important aspect of these columns is lack of specific physio-chemical interactions between the column material and the molecules being separated. The second type of retention mechanism is due to a chemical attraction between the solid column material and the molecule. Such columns can easily separate identically sized molecules such as toluene and o-xylene, for example. For our new inorganic clusters it is critically important to understand the mechanism of interaction with various column materials. These size exclusion columns are of two basic material types which we now discuss.

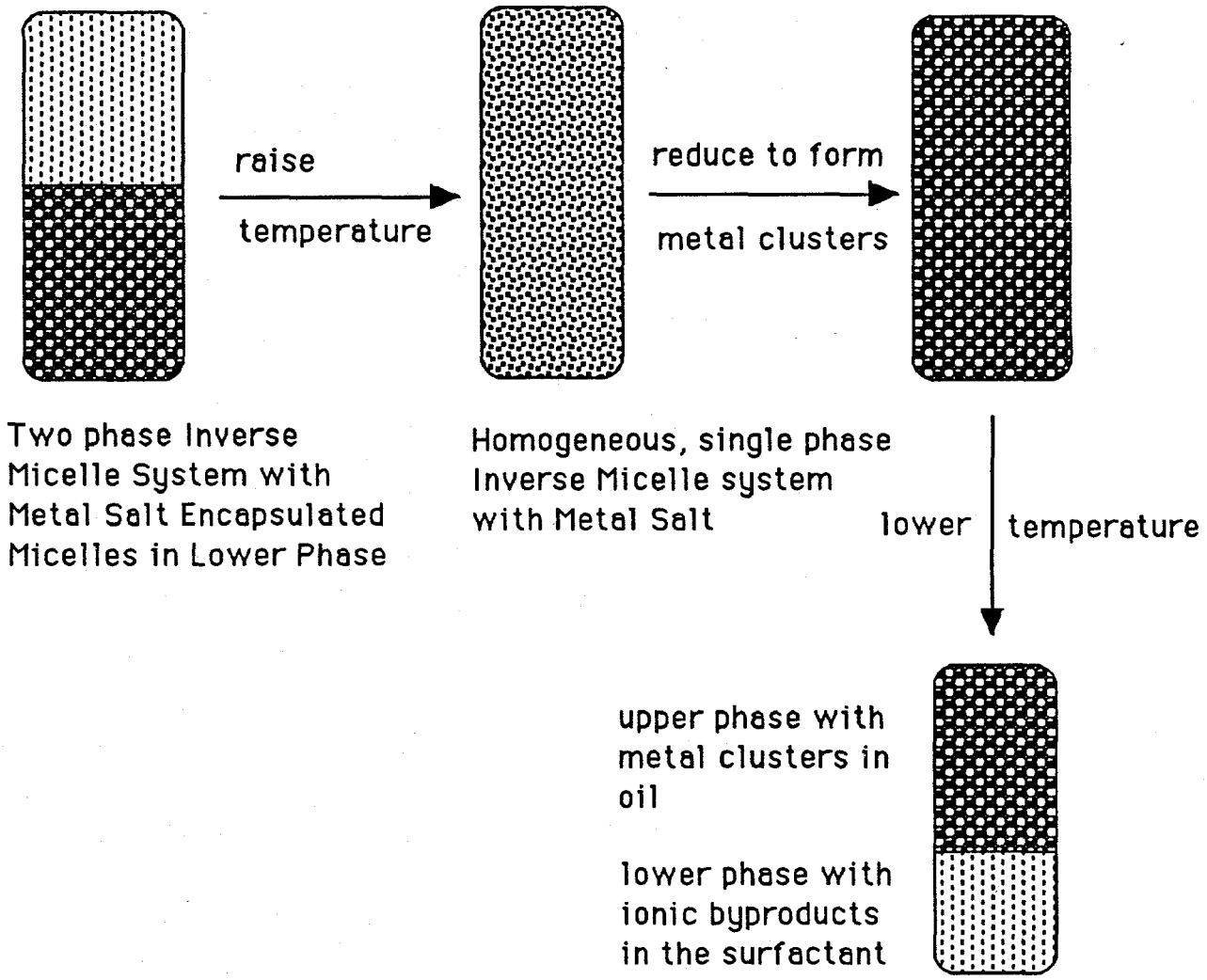

Figure 2. Scheme for separation of metal clusters from ionic byproducts using inverse micelle phase separation.

The first type of column has a porous gel (usually cross-linked microporous polystyene) packing with user selectable pore sizes from 50 Å to several hundred angstroms. For the clusters of interest to us either 50 Å or 100 Å porous gels were very effective in separating clusters whose molecular weight differences were only 5-10% (this corresponds to a variation of the cluster radius of only 2% for spherical clusters, a variation which would be totally impossible to measure by any other technique save mass spectrometry)! For example, a 50 Å porous column can easily separate decane from dodecane and many of our clusters elute at times which differ only slightly from these small molecules.

Calibration of these columns with molecules of known size was undertaken so that effective cluster sizes could be obtained from the retention time and compared to other measurements of cluster size such as TEM or light scattering. The results are shown in figure 3 for porous organic gel columns with the pore sizes indicated. All data were obtained with tetrahydrofuran (THF) as the mobile phase. Thus, we require our clusters to be stable in this coordinating organic solvent. Fortunately, this is true of all the layered semiconductor clusters tested, but it is not true of all the metal clusters (e.g. Au) and further development is required for purification of some of these. A significant feature to note is that either the 50 or 100 Å columns can distinguish hydrocarbon molecules which differ by only 2.5 Å in size. Thus, even with only a single 30 cm long column very good resolution of cluster size should be possible. By cascading 4 of these columns resolution of cluster size to ~2% should be possible. This is a wonderful (and very fast compared to TEM) new size characterization capability. We expected most of our clusters to have retention times between 5 and 10 minutes for these columns and this is indeed the case. The half widths of the eluting bands of our cluster solutions are often as narrow as monodisperse molecules such as hexadecane (c16) testifying to the excellent quality of the synthesized clusters.

The cluster-size distribution may be inferred by comparison of peak elution widths for perfectly monodisperse objects (e.g. for toluene the inherent instrument width is $\Delta t = .25$ min (full-width at half height), for a polymer standard with a weight average to number average molecular weight ratio (M_w/M_n) of 1.05 it is .36 min. In the chromatogram shown in figure 4 the main cluster peak is indistinguishable in shape and half-width from the monodisperse polystyrene standards used to calibrate the column.

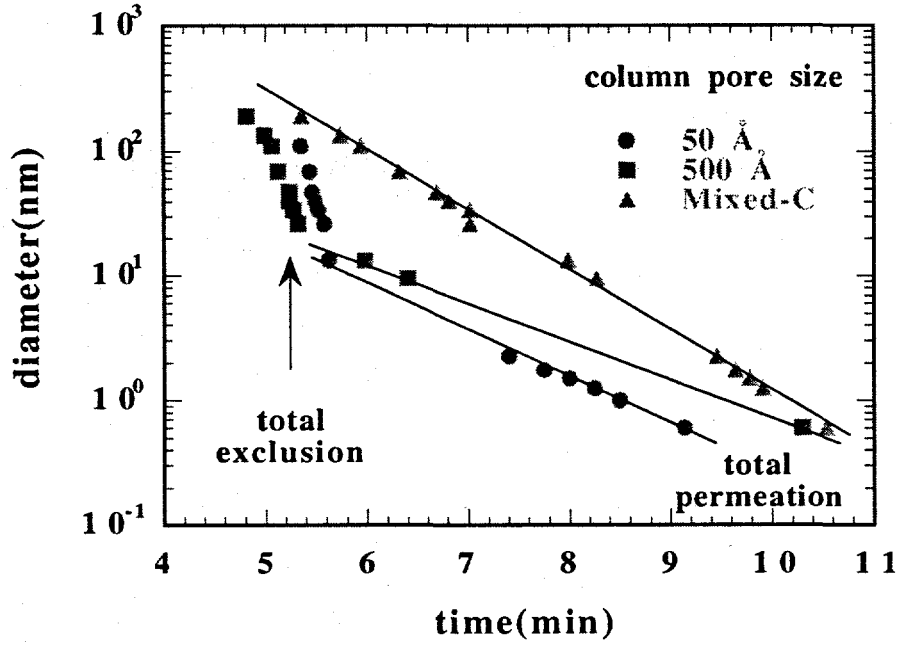

Figure 3. Calibration of size exclusion columns for use in cluster purification experiments. The mixed-C column has a variety of pores ranging in size from 100 Å to 2000 Å.

We actually are privy to much more information than simply the retention times which give us the average size of the cluster because the detector we use to monitor the peaks of figure 4 is a photodiode array which captures the spectrum from 190 to 600 nm for the entire peak in real time. This spectrum is free of all other chemical contributions and thus is truly representative of only these clusters. The purified cluster spectrum of MoS_2 is plotted along with that of the parent solution in figure 5. All the energies of the excitonic features are retained with many more details in the far UV revealed for the first time for the chromatographed sample. Similarly the fluorescence emission and refractive index changes accompanied by the passage of this group of monodisperse clusters is also obtained.

By chromatographing the same clusters on both types of columns we can learn much concerning both size distribution and surface structure of a population of clusters. Such information is not available by any other technique. It appears that many cluster properties are most easily studied by chemical techniques that are usually applied to gargantuan polymers such as DNA and proteins, as opposed to the methods of solid state physics. Polymers, too, can only be investigated with the aid of separation techniques

such as gel electrophoresis and chromatography. For clusters, neither purely chemical nor physical solid-state techniques by themselves provide complete characterization.

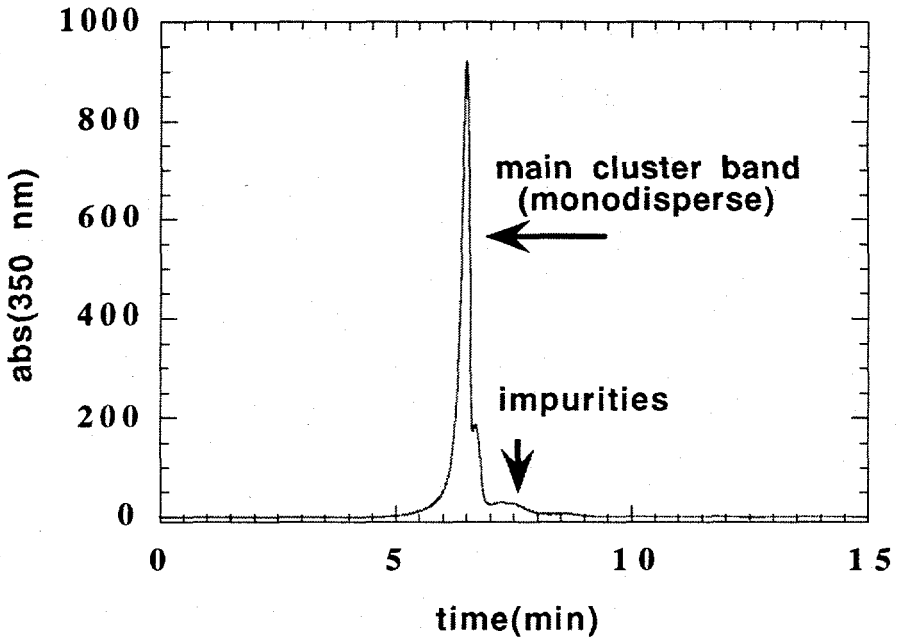

Figure 4. Chromatogram of the photodiode array (PDA) output at 350 nm vs time. The uv impurities may be detected with either the refractive index (RI) detector or the PDA output at 250 nm monitored by separate in-line detectors. Also, pesky fluorescent impurities found in nearly all samples elute at separate times from the clusters, allowing the inherent photoluminescence from the clusters to be determined.

A second type of chromatography column consists of packed spheres of porous silica with 100 Å-300 Å (user selectable) pore size and with user selected organic "bonded" phases. These phases can range from very hydrophobic such as c18 groups to c4 groups and even very hydrophilic groups such as diols and just bare silica. While a size exclusion mechanism similar to the first type of column described above is present, retention mechanisms in these columns, even for simple molecules of the same size, such as toluene and o-xylene, are very different and such molecules can be easily separated in time. The separation mechanism for such columns is best thought of as differential solubility in the solid phase of the column compared to the mobile phase. Only if there is no solubility (i.e. chemical interaction) at all in the bonded phase will these columns function with a strict size exclusion mechanism.

In figure 6 we show the effect of size on the absorbance onset for MoS_2 clusters synthesized by our technique and purified on a size-exclusion column. The retention time of each group is also shown, this quantity being proportional to the size of the

cluster in the absence of specific interactions The shift of the bandgap from ~520 nm to ~300 nm is a excellent example of the quantum confinement effect mentioned in the introduction.

The advantage of having detector information at a wide range of wavelengths at all times is particularly evident when identification of the cluster peak is desired. Of all the reaction byproducts only the clusters have absorbance which exceeds 300 nm so observation of the elution profile in both the UV (250 nm) and near the first exciton of the cluster (350 nm) as shown in figure 7 below reveals the presence of many impurities which separate nicely from the clusters. This separation explains our ability to observe the inherent optical features of the MoS_2 clusters as shown in figure 5.

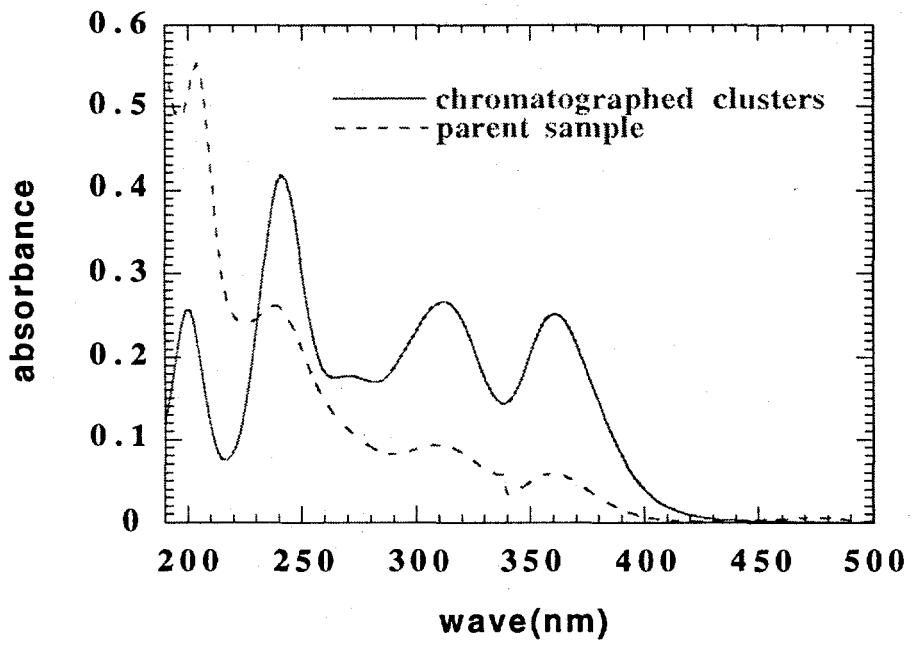

Figure 5. The MoS_2 cluster band of the previous figure is monitored on-line by a photodiode array which captures all the spectral features in real time during the chromatography. Note the additional details not resolved in the parent sample before purification.

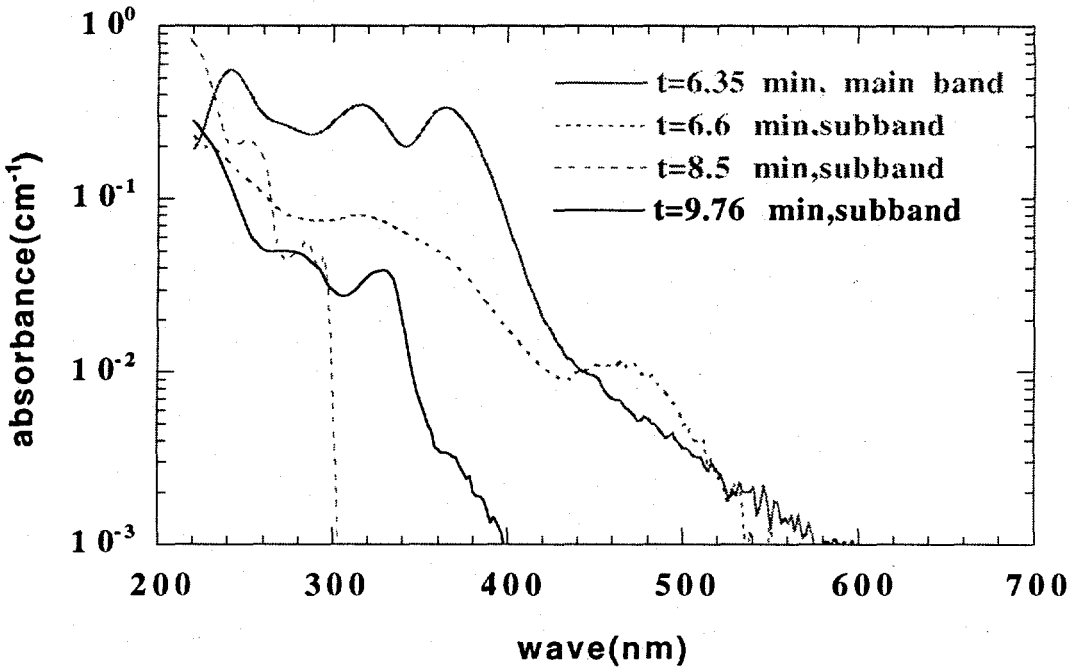

Figure 6. Size exclusion chromatography is used to separate small subpopulations of clusters with various band-edge absorbances from the main population of clusters. The shifts of the first excitonic peak from the bulk value are rather dramatic. The longest retained clusters at 9.76 min are very close in size to a toluene molecule (6-10 Å) and thus are truly molecular in nature, while the main band has a retention time comparable to a large surfactant molecule (i.e. 3 nm.). The average pore size of the column used is 100 Å and the carrier solvent is tetrahydrofuran (thf).

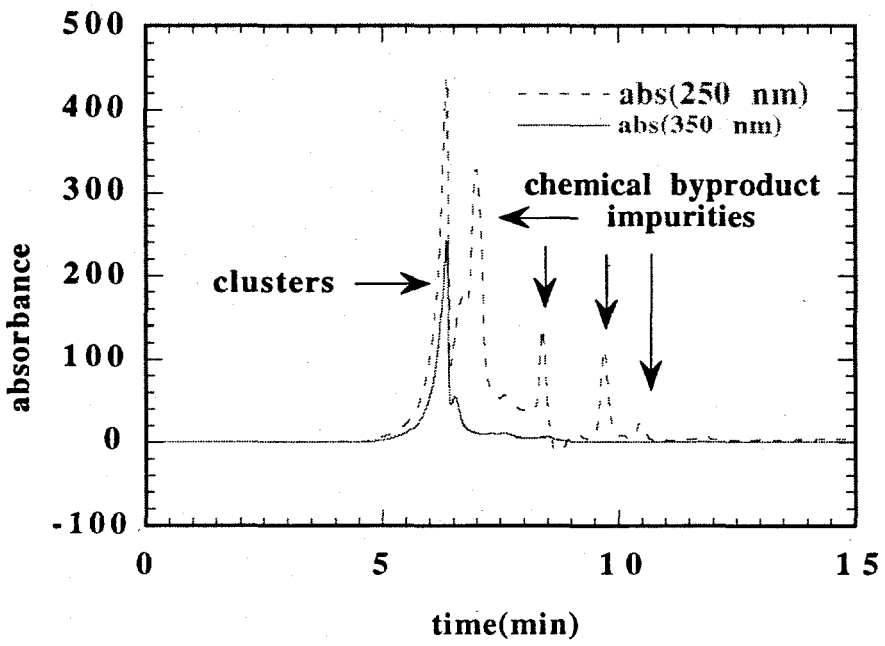

Figure 7. Extraction of the absorbance at 350 nm (clusters) from that at 250 nm (clusters and UV-impurities) shows where the clusters elute.

III. Optical Properties of Semiconductor Clusters: Strong Quantum Confinement Effects

Many of the most interesting physical properties of clusters are a consequence of the spatial confinement of their electrons, and much recent research is aimed at understanding the evolution of clusters properties with cluster size. Especially interesting are the manifestations of electron and hole confinement in semiconductor clusters as the cluster size decreases below the excitonic Bohr radius, and the electronic band structure gives way to discrete molecule-like electronic states. These effects have been studied experimentally and theoretically mostly in groups II-VI semiconductors (CdS, CdSe, CuCl, etc.) and to a much lesser extent in groups IV and III-V semiconductors (Si and GaAs) and other materials.[1,6]

We have synthesized and studied several semiconductor clusters (some for the first time) including MoS_2, WS_2, PbS and TiO_2. In this section we shall focus on MoS_2 as a model system. Our choice of MoS_2 was motivated by both applied and scientific interest. On the scientific side, bulk MoS_2 crystallizes in a hexagonal layered structure ($P6_3/mmc$-D^4_{6h}) composed of sheets of Mo atoms sandwiched between sheets of S atoms in a S-Mo-S arrangement. The S-Mo-S sandwiches are held together by weak van der Waals forces and are stacked along the c-axis with two sandwiches per unit cell (c=12.3 Å). Given this interesting layered structure and a novel synthesis method in which clusters are grown inside inverse micellar cages,[2,3] a number of questions were of interest: will clusters of MoS_2 in the <10 nm size range form? Can the size of such clusters be controlled? Will these clusters exhibit novel properties and strong electron confinement effects?

MoS_2 has numerous applications as a catalyst. For example, we are interested in the potential of MoS_2 as a hydrogenation catalyst for the conversion of coal to liquid fuels and as an electrode material for photoelectrochemical solar cells. In the latter application MoS_2 is expected to be highly stable against photo corrosion, and in both applications, clusters have significant advantages over bulk material.

The significant and as yet not understood feature of MoS_2 and WS_2 is the way the two-dimensional structure of these materials influences the electronic properties. Because of this anisotropy a relevant and important question is which dimension controls the quantum confinement effects in these materials? The transverse cross-section as measured by both size-exclusion chromatography, light scattering and TEM or the

thickness of the nanocluster? In fact, the careful reader will note from the previous figure 6 that the second MoS_2 cluster band at 6.6 minute actually has a lower energy exciton than the one at 6.35 nm. A strict interpretation of the shorter elution time as representative of larger overall cluster volume, (the characteristic which controls the elution time and makes larger objects elute earlier than smaller ones), would suggest that the thickness of the clusters at 6.35 minutes might be less than those at 6.6 minutes, but have a larger cross-section and a larger overall volume. The question is particularly relevant since recent STM measurements by our collaborator David Kelley at Colorado State have indicated some clusters are only one sandwich layer thick but are significantly larger in the orthogonal directions.

A. Synthesis and Characterization of MoS_2 Clusters

The clusters for the optical studies were grown inside inverse micellar cages in non-aqueous solvents. MoS_2 clusters are formed by first dissolving a molybdenum (IV) halide salt inside the surfactant cages (both nonionic and cationic surfactants may be used) and then combining this solution with another inverse micelle solution containing a sulfiding agent (e.g., metal sulfide or H_2S). All preparations were done in a Vacuum Atmospheres dry box with catalytic oxygen and water removal to prevent degradation of the Mo (IV) salt precursor. Both oxygen and water levels were monitored and kept below 1 ppm during the reaction. The Mo:S ratio was chosen to be 1:2 or less.[3] Beautifully clear suspensions varying in color from nearly colorless for the smallest clusters (< 2 nm in diameter) to deep blue for the larger clusters (~ 15 nm) are obtained. The cluster size is varied by using different sized micellar cages to encapsulate the Mo salt. These cluster suspensions are remarkable for they are homogeneous, stable and transparent dispersions of MoS_2 clusters in a non-polar fluid. When the reaction stoichiometry exceeds 2:1 in S:Mo then electron diffraction and x-ray diffraction show the expected bulk hexagonal structure as shown in the selected area diffraction (SAD) pattern of figure 8. High resolution TEM (HRTEM) lattice fringe images of 3.2 nm MoS2 reveal excellent crystalline order and lack of point and line defects as shown in figure 9. However, studies of structure on clusters with sizes less than 3 nm are very difficult as there are simply not enough atoms in bulk lattice positions to give a significant diffraction signal, nor many reflections. Thus, the structure of the smallest, molecular-like clusters remains unresolved.

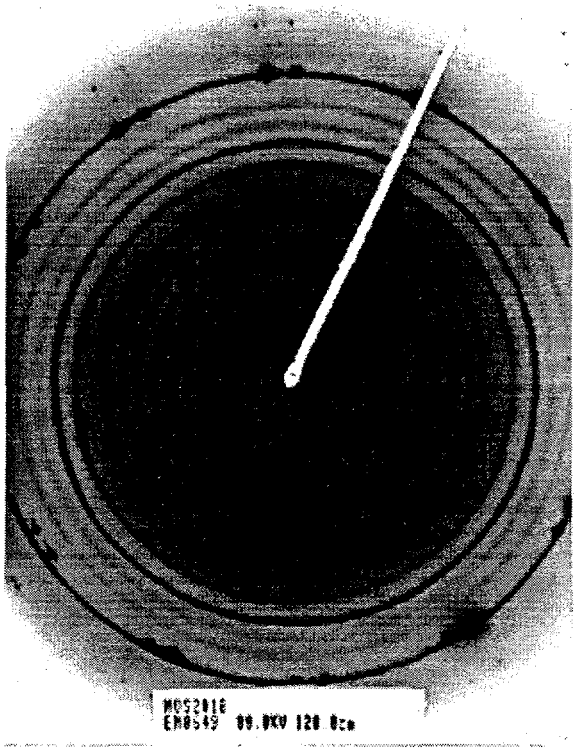

Figure 8. SAD of 4.5 nm MoS_2 clusters grown in an inverse micelle solution shows the broad diffuse rings and lattice symmetry expected for a hexagonal structure.

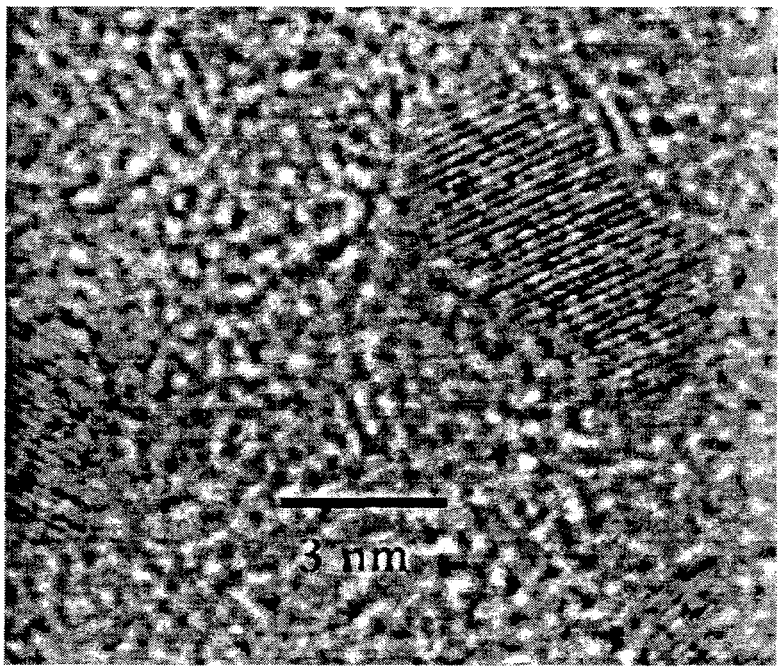

Figure 9. High resolution image of 3.2 nm MoS_2 clusters shows the excellent crystal order and lack of point and line defects.

B. Optical Properties and Physics of MoS_2 Clusters

Figure 10 shows the optical absorption spectra of 4.5 nm and 2.5 nm diameter MoS_2 clusters dispersed in acetonitrile at concentrations of ~10^{-3} molar and compares the results with those of bulk single crystals (inset). These spectra, which were measured at 290 K, exhibit well-defined features which we now wish to discuss.

First we review briefly the spectrum of bulk MoS_2. This spectrum, which has been studied extensively[7,8] and compared with results of electronic band structure calculations,[9] consists of a series of absorption thresholds. The first threshold corresponds to weak absorption in the near IR at ~1040 nm (~ 1.2 eV) (not shown) associated with an indirect gap between Γ and the middle of the Brillouin zone between Γ and K. The second threshold occurs at ~ 700 nm and is associated with a direct transition at the K point. The two sharp peaks (A and B) on the high energy side of this threshold are excitonic transitions (K_4~K_5 and K_1~K_5, respectively) whose energy separation (~0.18 eV) is due to the spin-orbit splitting of the top of the valence band at the K point.[9] A third threshold at ~ 500 nm is due to a direct transition (specifics unknown) from deep in the valence band to the conduction band. Excitonic features (C and D) are also associated with these transitions. A fourth threshold at ~ 350 nm is also due to transitions from deep in the valence band. Features on the high energy side of this threshold (labeled X our own notation, and E in Fig. 10) are seen in thin samples. The relative intensities of peaks A and B, C and D, and X and E are known to vary with sample thickness as well as quality.[7,8]

The spectrum of the 4.5 nm clusters in Fig. 10 is rich in spectral features, the most prominent of which we have labeled 1 through 5. Multiple maxima in the absorption spectra of clusters can be due to either specific electronic transitions in monodisperse clusters or to the presence of structured size distribution (e.g., magic numbers) of clusters in a given sample. In the present case, however, comparison of spectra on several samples shows no evidence for structured size distributions, and thus the features in the spectrum are intrinsic properties of monodisperse clusters and attest to the high quality of our clusters. The clusters are highly crystalline with little or no lattice defects as shown in the higher resolution TEM of figure 9.

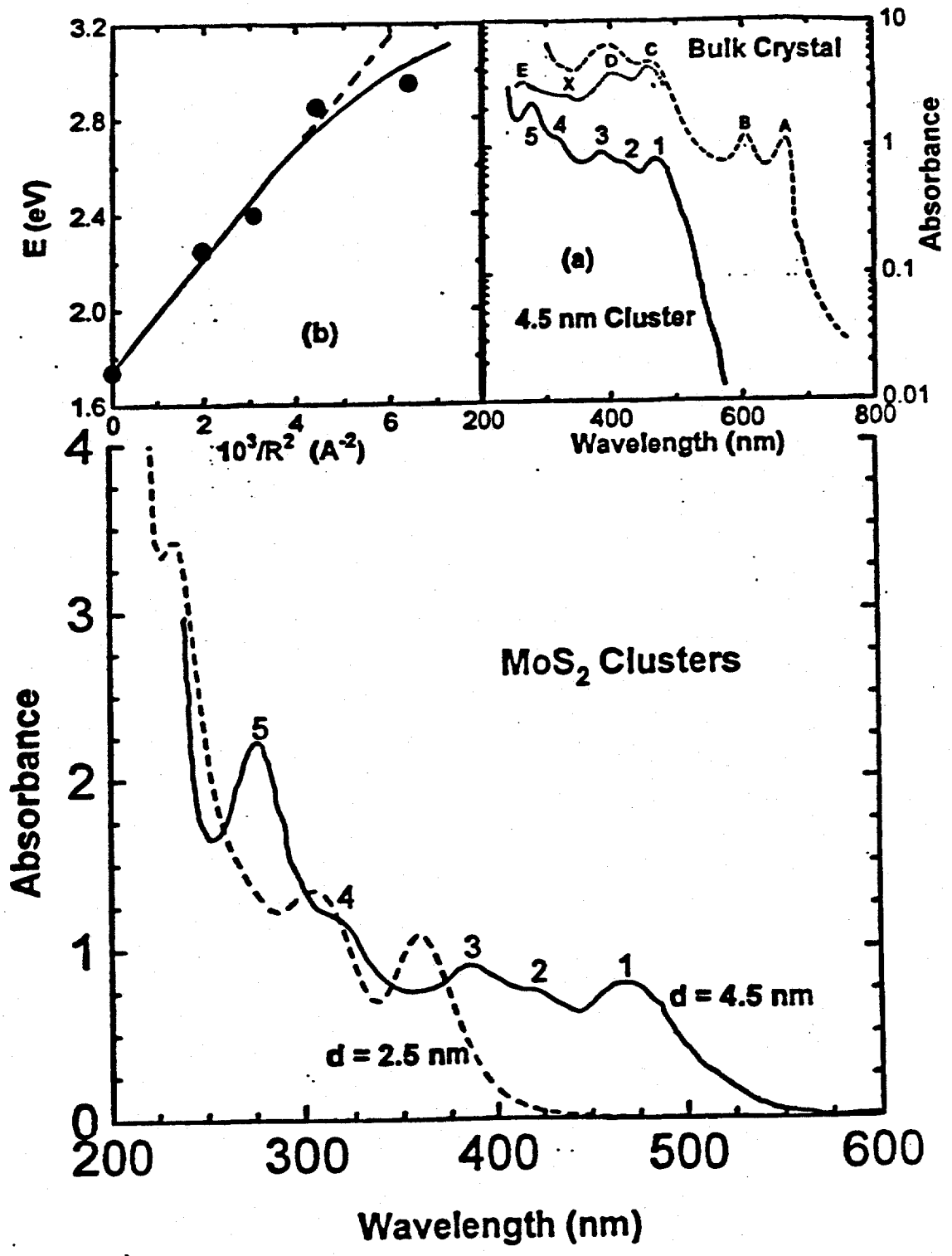

Figure 10. Optical absorption spectra of 4.5 and 2.5 nm MoS_2 clusters (absorbance in arbitrary units). Inset (a) compares the spectrum of the 4.5 nm clusters to that of bulk thin (dotted) and thick (dashed) crystals (Refs. 7 and 8). Inset (b) shows the dependence of the absorption threshold at the K point on cluster size.

Comparison of the spectrum of the clusters to that of the bulk crystal reveals two main features: (1) a large blue shift for the clusters, and (2) preservation of the excitonic features in the spectrum of the clusters. In fact, a detailed comparison of this spectrum to that of the bulk crystal allows an essentially one-to-one association of the features in both spectra (inset Fig. 10). First, it seems certain that feature 1 (λ = 470 nm) in the cluster spectrum is associated with excitonic peak A (λ = 665 nm) of the bulk, corresponding to a blue shift of 0.78 eV due to the quantum size confinement effect of the 4.5 nm clusters. If we then, as a rough approximation, assume that all of the other peaks of the bulk crystalline spectrum are blue shifted by the same amount, then their energies in eV(nm) would be: B=2.86 (434), C=3.45 (360); D=3.90 (318), X=4.50 (276), and E=5.30 (234). For comparison, features 2, 3, 4, and 5 in the spectrum of the 4.5 nm clusters have energies of: 2.92 (425), 3.24 (382), 3.92 (317) and 4.51(275),respectively. It is seen that these latter energies are close to the expected shifted positions of peaks B, C, D and X (the biggest difference being for peak C), thereby providing an argument for the one-to-one association of these features. Our assumption that all the peaks in the single crystal spectrum blue shift equally in energy upon going to the clusters cannot, of course, be strictly correct as different parts of the band structure (or Brillouin Zone) should be affected differently by quantum size confinement due to differences in effective masses. In reality, however, the above analysis shows that this assumption is not far wrong for MoS_2 which implies, in the context of simple models, that the effective mass must not vary strongly among the various points of the Brillouin Zone involved in the observed optical transitions. Despite any uncertainties in the above association of spectral features, the important point we wish to make is that the absorption spectrum of the 4.5 nm clusters is essentially bulk like.

The above conclusion that features 1 to 5 in the spectrum of the 4.5 nm clusters derive from features in the bulk single-crystal spectrum is consistent with the fact that these clusters are somewhat larger than the size of the exciton (radius r_B=2.0 nm) in bulk Mos_2. For these clusters there are apparently sufficiently high densities of states in the conduction and valence bands to make it possible to produce bulk band-like features in the absorption spectrum and thereby preserve the quasiparticle character of the excitons. Thus, the spectrum of the 4.5 nm clusters reflects in a beautiful manner size quantization of excitonic features in the weak-to-moderate confinement regime (cluster radius R > r_B).The above results also strongly indicate that 4.5 nm MoS_2 clusters retain the bulk hexagonal crystal structure of this material.

Turning next to the spectrum of the 2.5 nm clusters in Fig. 10, we note that this spectrum is qualitatively different from that of the 4.5 nm clusters and of the bulk crystal.

Specifically, on going to the 2.5 nm, clusters, the excitonic features in the spectrum give way to a ladder of three well-defined peaks over the spectral range covered. This is the expected behavior in crossing over from the weak (excitonic) confinement regime to the strong (non-interacting carrier) confinement regime where the cluster size (in this case R =1.25 nm) is considerably smaller than the excitonic Bohr radius (r_B = 2 nm). For these very small clusters the low densities of states prevent observation of excitonic features, and the allowed energy levels change from continuous bands to a ladder of essentially discrete levels as in molecular systems as shown in figure 11. Figure 12 shows that the spectrum of 3.0 nm MoS_2 clusters is very similar to that of the 2.5 nm clusters reflecting this ladder of discrete levels. This result indicates that the crossover from solid-like to molecule-like behavior occurs at a cluster size between 4.5 and 3.0 nm. Comparison of the spectra in Figs. 10 and 11 shows only relatively small blue shifts of the absorption peaks in going from 3.0 to 2.5 nm clusters. This trend was manifested by a third sample with 2.0 nm clusters. Thus, it appears that the absorbance blue shift levels off in this (3 - 2 nm) size range.

That this leveling-off in the shift occurs in the size range where the clusters become molecule-like is not surprising and strengthens the assertion that the optical properties of these clusters are indeed molecule-like. The ladder of peaks in the absorption spectra of the clusters in this size range then corresponds to transitions to various excited molecular states with some vibrational broadening as illustrated in figure 12. We note here that a qualitatively similar leveling-off in the blue shift has been reported for small PbS clusters in what is also believed to be the molecular range.

A variety of theoretical models have been used to describe size quantization of the energy spectrum of the carriers in semiconductor clusters. These models, which express the size dependence of the energy of the excited states in terms of the bulk energy gap, the kinetic energy, Coulomb interaction and correlation energy of the electron-hole (e-h) pairs, have been recently reviewed by Yoffe.[6] They include the initial effective mass (EM) treatment of Efros and Efros[10] and later improvements by Brus,[11] Kayanuma[12] and others, semi-empirical tight binding treatments and recent empirical pseudo potential methods. Despite their shortcomings, the EM models contain some of the essential physics and provide a qualitative framework for examining experimental data and their trends. In terms of these models, and in the size regime where quantum confinement effects are prominent, the shift of the absorption edge, or bandgap, E(R) of a cluster of radius R relative to that of the bulk is to a reasonable approximation proportional to $1/2\mu R^2$ where μ is the reduced mass of the exciton.[13,14] A plot of E(R) vs. $1/R^2$ should then yield a straight-line with slope a $1/(2\mu)$. Such a plot for the

sharp absorption threshold at the K point of the zone (E_g-1.74 eV in the bulk) for our clusters is shown in the inset of Fig. 10 and is linear for clusters larger than 3 nm in diameter. The linear portion yields $\mu = 0.16\ m_0$,where m_0 is the free-electron mass. Interestingly, this value compares favorably with the bulk value of the reduced mass of $0.18\ m_0$ for the A exciton deduced from optical measurements along the optic c-axis of the crystal.[8] While we cannot rule out the possibility that this agreement between the two values of μ may be fortuitous, it suggests that simple EM models capture some of the essential physics for MoS_2 clusters.[13]

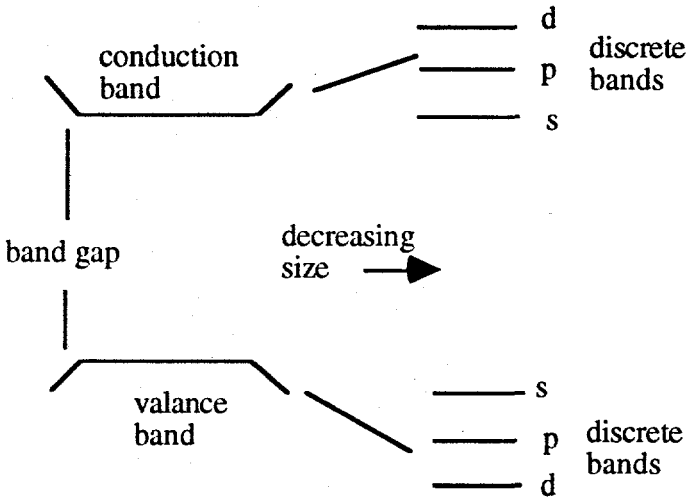

Figure 11. Continuous bands become discrete while valance and conduction band edges change energy as the cluster size decreases. The structured features in the spectra of the 2.5 and 3.0 nm clusters in Figures 10 and 12 are due to the discrete nature of the optical transitions in small clusters.

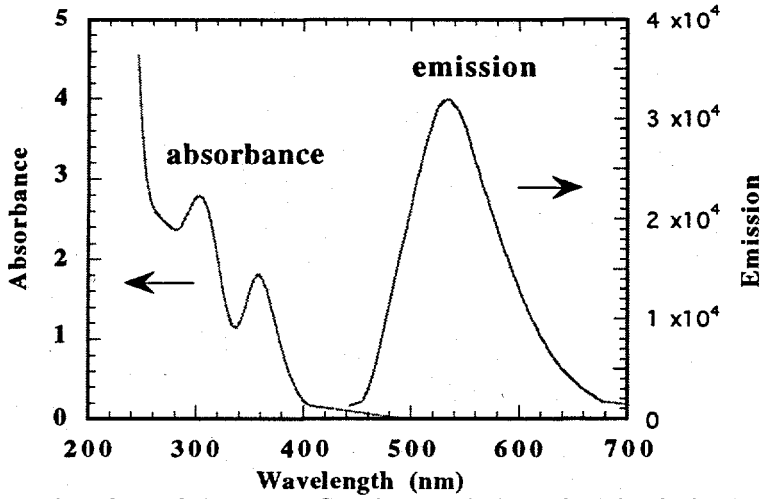

Figure 12. Photoemission from 3.0 nm MoS_2 clusters is broad and relatively weak and occurs primarily from trapped surface states. Little difference in the absorbance or photoemission is observed compared to the 2.5 nm clusters of figure 10.

Figure 12 also shows the room temperature emission spectrum for the 3.0 nm diameter clusters excited at 476 nm. In this early study we did not observe any luminescence due to direct e-h recombination near the absorption threshold for any of the clusters. Rather, the spectrum consists of a blue-shifted (relative to bulk emission), broad emission peak centered at 537 nm which is characteristic of surface and/or defect recombination. For these 3.0 nm clusters many of the atoms lie at or near the surface, the surface states associated with adsorbed species dangling bonds and other defects can be expected to play a major role in determining the fate of the carriers produced by light absorption.

A significant issue in studying the photoemission and photoexcitation behavior of nanoclusters is the role of solvent impurities in the observed spectra. The spectrum in figure 12 was obtained on as-synthesized MoS_2 clusters with all the chemical byproducts of the synthesis still present. To investigate these clusters further, we purified the clusters by chromatography and then trapped them on-line in our fluorescent detector. We then scanned both the photoemission as a function of excitation wavelength and the photoexcitation while monitoring the peak of the photoemission.

The results of such experiments are shown in figures 13 and 14 and reveal several features which had not been observed previously in these clusters. First, we confirmed that the photoemission observed in figure 12 was inherent to the clusters and

not an artifact of chemical impurities. The spectrum shown in figure 13 shows photoemission at 520 nm as observed in the parent solution. In the photoexcitation spectrum shown in this figure we observe discrete features in the UV which could not be observed in the parent solution, both due to strong UV absorbance effects in this solution and the fact that the excitation lamp of our SPEX spectrometer cuts off at 250 nm.

We then performed photoemission experiments in which we excited at the discrete wavelengths observed in figure 13 (specifically 225 and 245 nm). The 225 nm excitation results, shown in figure 14, reveal photoemission from deeper states in the bandgap and show a distinct shoulder to longer wavelengths. These observations indicate that a wide range of energies of either hole or electron traps exists at the surface of nanoclusters and, since the clusters are chromagraphically pure, rule out the possibility of such different traps originating in sample polydispersity.

The implication of these observations for applications such as photocatalysis is that sites exist on identically sized, purified MoS_2 clusters whose valence and/or oxidation potentials can effect a wide variety of chemical reactions. This is true even though these clusters have only a single, well-defined bandgap for exciton creation. It is interesting to speculate that the disc-like layered nature of nanocluster MoS_2, which inherently provides for both edge and top/bottom-surface sites, is responsible for this possibility. Further studies on non-layered materials such as CdS or PbS would settle this questions more thoroughly. Indeed, preliminary studies of both of these materials as part of another LDRD project fail to show the photoemission complexity observed in these layered materials.

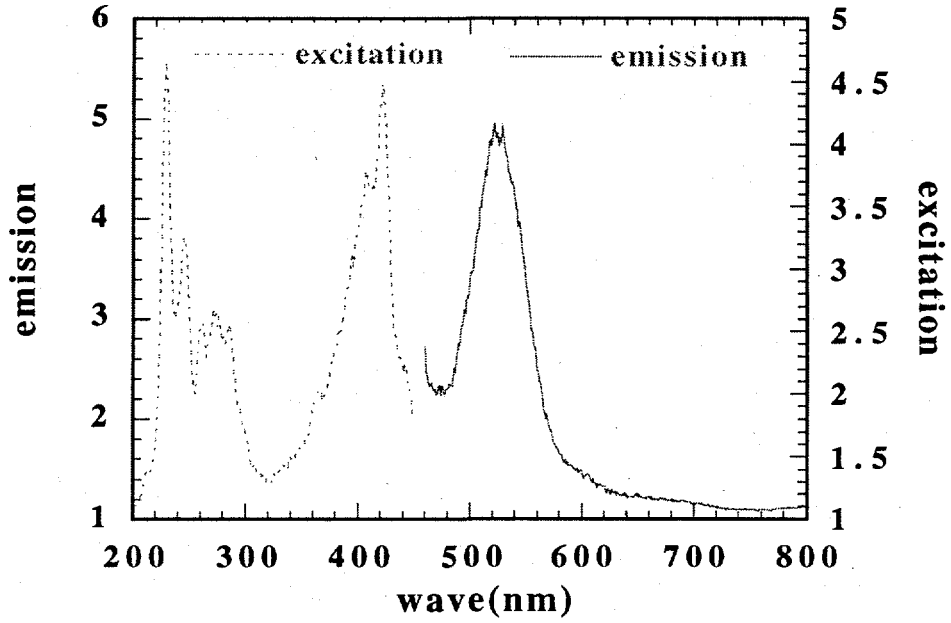

Figure 13. The photoemission and photoexcitation of 3.0 nm MoS2 clusters which have been chromatographically purified and trapped on-line in our fluorescence detector. The emission was obtained using 425 nm excitation, while the excitation was scanned at the emission peak of 520 nm.

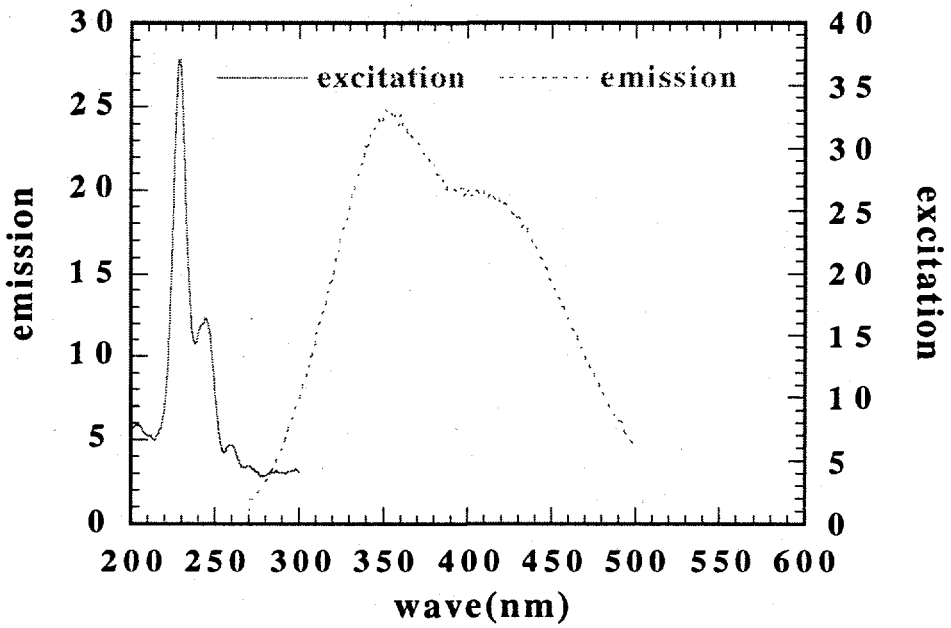

Figure 14. The photoemission of chromatographically purified 3.0 nm MoS_2 clusters when excited at 225 nm is very different than observed in figure 13.

Finally, given the layered nature of the MoS_2 structure, it is interesting to speculate about the shape of MoS_2 clusters in the size range of the present study. In its hexagonal phase, the unit cell of MoS_2 contains 2 formula units and has dimensions a=3.15 Å and c=12.30 Å yielding a unit cell volume = 317 $Å^3$. Assuming spherical clusters and full packing, a 4.5 nm diameter cluster would contain 150 unit cells, or 300 formula units, and a 2.5 nm diameter cluster would contain 26 unit cells, or 52 formula units. However, the shape of the unit cell precludes full packing, and so the number of molecules in these clusters can be expected to be considerably less. As noted above, the 4.5 nm clusters appear to retain the bulk structure, and in a spherical box these clusters will be ~ 4 unit cells thick. We do not know the structure of the 2.5 nm clusters, but this size is equivalent to 2 unit cells thick. However, it is not likely that these small clusters will have any strong semblance to the bulk structure since a stack of two unit cells does not define a structure, additionally, as already noted, the optical spectrum of these clusters reveals their molecular character. In all cases we envision the clusters to be disk shaped.

In conclusion, highlights of our work on MoS_2 quantum confinement include the observation of: 1)remarkable structure in the absorption spectra reflecting the underlying physics as well as the high quality and size monodispersity of the clusters; 2) large blue shifts in the spectral features with decreasing cluster size affording great tailorability of the bandgap; and 3) a beautiful demonstration of the crossover from band-like (solid) to molecule-like spectra as the size of the clusters becomes smaller than that of the exciton in the bulk.

C. Other Layered Semiconductor Clusters

Although we have not performed as extensive investigation of the other layered semiconductor materials such as $MoSe_2$, $MoTe_2$, WS_2, and WSe_2, the optical features and size dependent bandgap shifts noted for the MoS_2 also appear to hold for these systems. In addition, the synthetic and processing techniques employed for MoS_2 also pertain to these systems. All layered systems investigated show the structured spectra found for MoS_2. For example, WSe_2 clusters show the same types of optical features as MoS_2 as shown in figure 15. Furthermore, a high degree of crystallinity is found as shown in the high resolution lattice fringe image of figure 16.

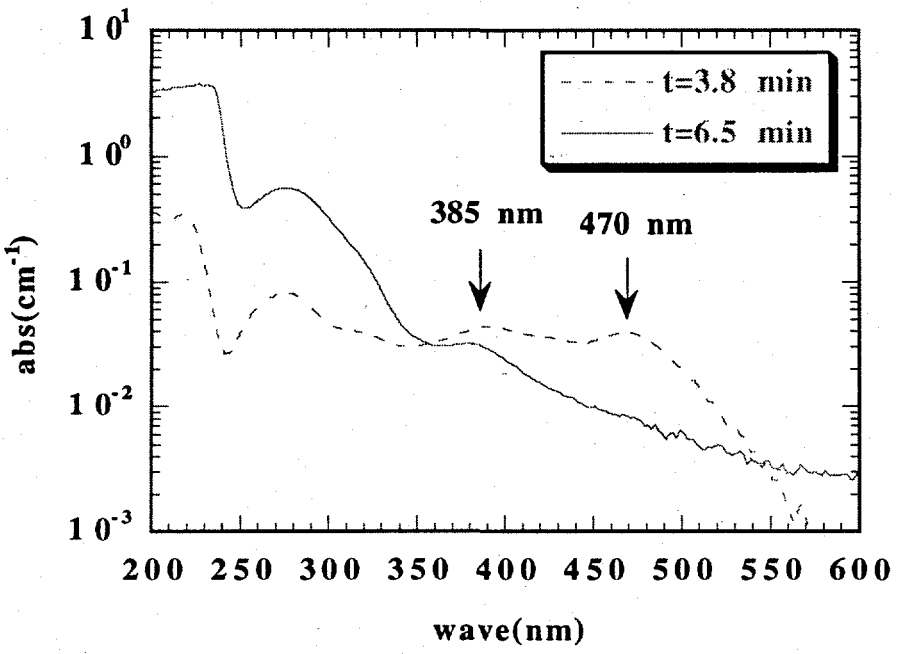

Figure 15. WSe_2 clusters processed by size exclusion chromatography. The larger (shorter retention time of 3.8 min) yellow colored clusters with an excitonic peak at 470 are shown in the high resolution TEM of the next figure. The more strongly retained, smaller clusters (t=6.5 min) with a first exciton at 385 are nearly clear in color due the strong quantum confinement.

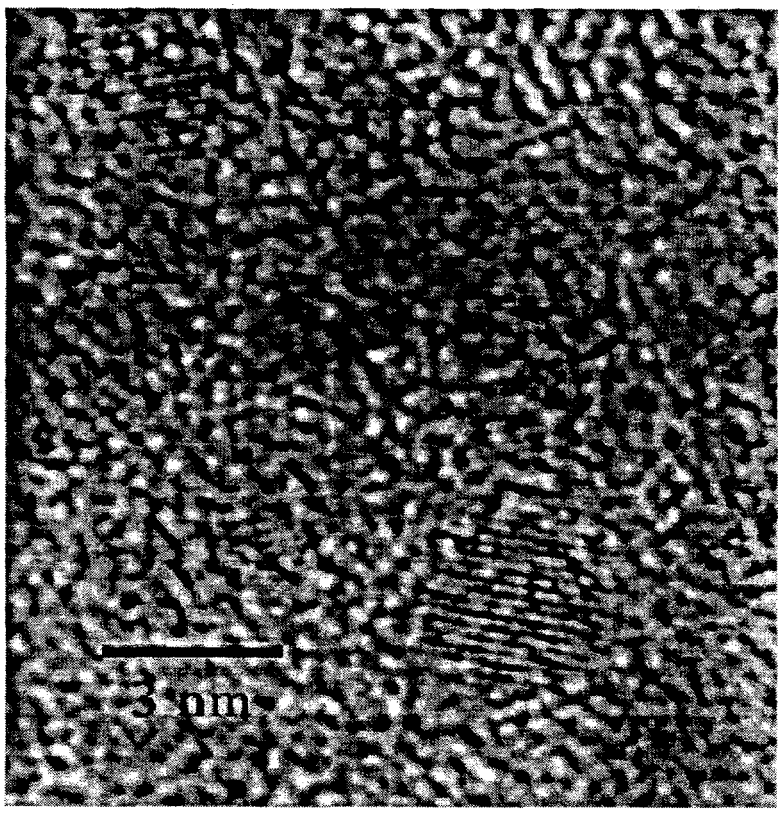

Figure 16. High resolution lattice fringe image of the larger WSe_2 cluster in Figure 15.

IV. Magnetic Properties of Metallic Clusters

The properties of nm-sized magnetic particles have been studied both experimentally and theoretically for more than sixty years.[15-18] Interest in these materials has remained high because of their potential use in numerous practical applications in magnetic recording, magnetic fluids, permanent magnets and catalysis. In addition, there are fundamental research questions concerning the development of long-range magnetic order and associated hysteretic properties such as coercivity and remanence as the cluster size increases from a few atoms with all atoms at the surface to a large cluster with predominantly interior atoms. Cluster synthesis and experimental handling play crucial roles in understanding the magnetic properties, particularly in separating the intrinsic properties from the effects of a surface layer[19-22] (such as a thin oxide shell) or particle-particle interactions due to agglomeration [22]. Iron was chosen as our model system because it is inexpensive and has broad potential applications as well as having been a subject of earlier study. We have also synthesized Ni and Co nanoclusters and initiated preliminary studies on them; however, we shall concentrate on Fe clusters in this report.

Progress in the study and utilization of magnetic clusters has been severely hampered by the lack of synthetic approaches for producing pure monodisperse clusters. Here, we report initial studies on the magnetic properties of α-Fe clusters prepared by a novel synthesis technique which yields monodisperse particles and, we believe, mitigates both surface layer and agglomeration effects. Following are synthesis, microscopy and experimental details, presentation of the magnetic properties and concluding remarks placing our results in context.

A. Synthesis and Size Control of α-Fe Clusters

Three conditions can be used to control the final cluster size: the micelle size, intermicellar interactions (e.g., phase boundaries which determine micelle diffusion rates) and reaction chemistry. To provide a constant magnetic background independent of cluster size, we have employed a single type of surfactant and solvent and varied the reduction chemistry to control the final iron cluster size for the experiments described here. We varied the strength of the nonaqueous reducing agents used to reduce the Fe(III) to Fe(0) so that the most rapid reduction kinetics produced the smallest final iron

clusters. Size-selected α-Fe metallic clusters with diameters between 1.4 and 15 nm were produced.

Spectroscopy was used to demonstrate 100% reduction of the Fe(III) to the final Fe(0) cluster form. All reactions took place in anaerobic conditions in a Vacuum Atmospheres dry box with continuous oxygen and moisture removal and appropriate sensors. Typical oxygen levels were 0.1 to 1 ppm and moisture levels were 0.5 to 3 ppm in the dry box. All solvents and surfactants used were high pressure liquid chromatography (hplc) grade and were completely dust free. The latter is critical to prevent inhomogeneous nucleation. Magnetization samples were weighed to determine total iron concentration and transferred to capped NMR tubes in the dry box to minimize oxygen exposure. The capped tubes were then removed from the dry box and transferred to the commercial SQUID magnetometer (Quantum Design MPMS) for magnetic characterization.

The inverse micelle system used in these experiments was DTAC (dodecyltrimethylammonium chloride) in hexadecane with hexanol used as a cosurfactant. Previous small-angle neutron scattering has shown that this system provides stable growth in the cluster size range of 1 to ~18 nm which was well suited to the present investigation. After growth occurs, the resulting clusters are fully dispersed and stable in a variety of oils and their magnetic properties may be investigated as a function of cluster size. The stability against agglomeration is due to the presence of the surfactant on the cluster surface.

The cluster formation reaction can be followed by the changes in the solution absorbance spectra upon addition of the reduction agent. Figure 17 shows the initially transparent, yellow colored micellar solution (labeled pre, for precursor) which has three charge transfer bands due to ligand complex formation of the surfactant micelle with the Fe(III) salt. It is quite interesting to note that these spectral features are quite different in energy from those of the same salt when dissolved in water or a polar organic solvent such as thf which implies a possible change in the reduction kinetics in these media which might affect final cluster size or morphology. This is illustrated in figure 18. Upon addition of the super hydride reducing agent, (essentially an organic source of H^- ion), reduction of Fe(III) to Fe(0) occurs with the liberation of H_2 gas. Obviously, at least a 3:1 molar ratio of this reducing agent to $FeCl_3$ precursor is needed for 100% reduction to iron clusters. For example, one can see from figure 17 that a 1:1 stoichiometry (squares) fails to remove all the Fe(III) from solution, while the other reactions all result in complete reduction with the appearance of a clear to yellow solution with broad absorbance. The latter is actually due to weak light scattering, as Fe(0) has

no inherent absorbance in the visible. The extent of light scattering, in fact, is a rough measure of the final particle size.

Figure 19 is a bright field transmission electron micrograph (diffraction contrast) taken on a JEOL1200EX at 120 kV showing the isolated, monodisperse 12.5 ± .5 nm Fe particles formed in one synthesis (the scale is indicated by the 20 nm bar).

Selected area electron diffraction confirmed that these particles have the bcc α-Fe phase. Other monodisperse α-Fe clusters produced by this surfactant/solvent process ranged from 1.4±0.1 to 15.0±0.5 nm, all below the maximum size of 16.4 nm [24] for single magnetic domain Fe.

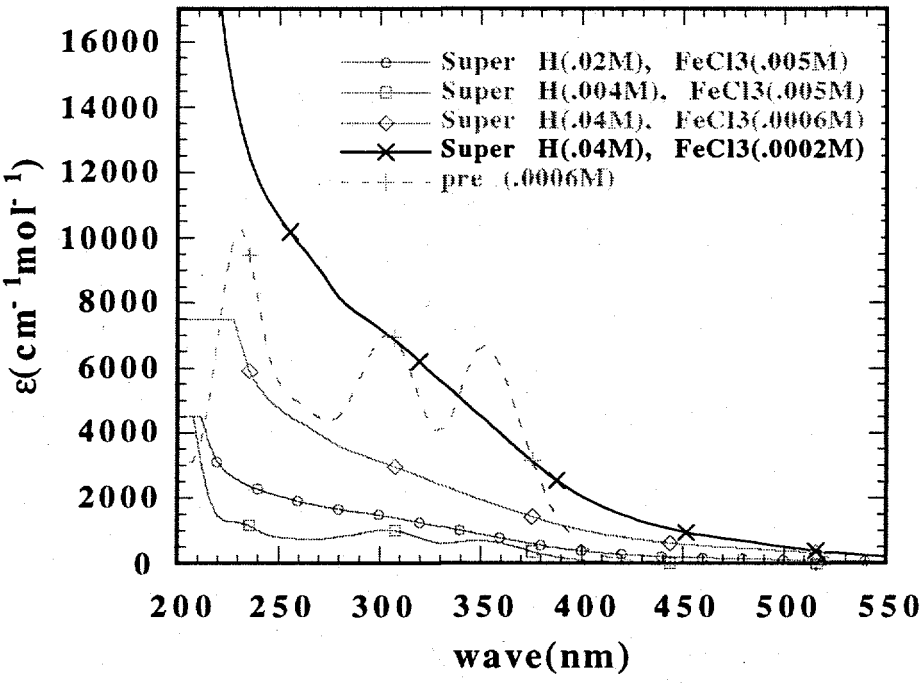

Figure 17. Effect of ratio of reducing agent, (superhydride) to precursor salt, $FeCl_3$, on the final solution optical absorbance. Incomplete reduction results in some Fe(III) as shown in the second case (square symbols).

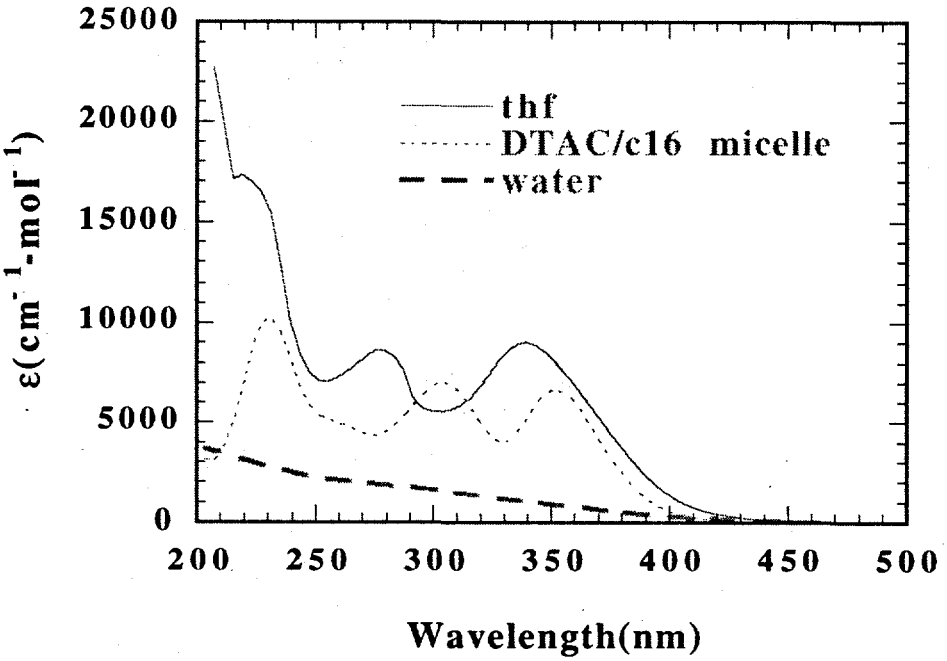

Figure 18. Effect of ligand coordination on the energy levels of a charge transfer complex of $FeCl_3$ in continuous and micellar media.

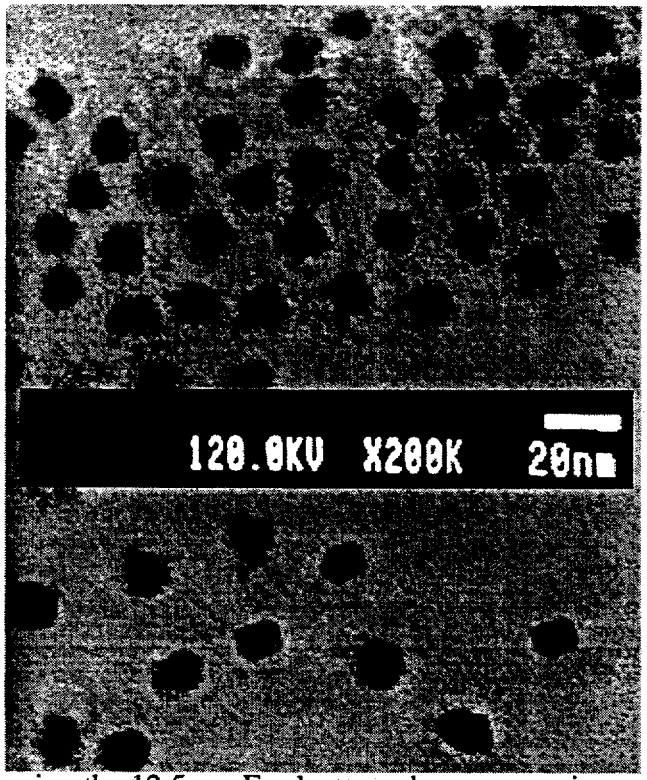

Figure 19. TEM showing the 12.5 nm Fe clusters whose magnetic properties were investigated.

B. Magnetic Properties of α-Fe Clusters

Figure 20 compares the response to an applied magnetic field at 5 K for the dissolved $FeC1_3$ salt (Fe(III) ions in a frozen solution) before adding the reducing agent (open triangles) to that of 12.5 nm Fe clusters after reduction (solid triangles). The dashed line is a Brillouin function fit to the Fe^{+3} ion data using a g-factor of 2 and an angular momentum of 2.5. The agreement confirms the presence of isolated Fe^{+3}; further, the low-field slope (susceptibility) decreases by a factor of 2 between 5 and 10 K, suggesting negligible magnetic interactions between the ions. In contrast, the Fe clusters show a distinct saturation in their response for fields above 1 tesla, consistent with ferromagnetic or superparamagnetic behavior characteristic of strong magnetic interactions within the clusters. Note the qualitative difference between the isolated ions and the clusters: the isolated Fe^{+3} ions exhibit a linear response to applied field at low fields and a nonlinear response at high fields while the 3.7 nm Fe clusters show a nonlinear response (and a larger moment per gram) at low fields but saturate to a constant moment in moderate fields.

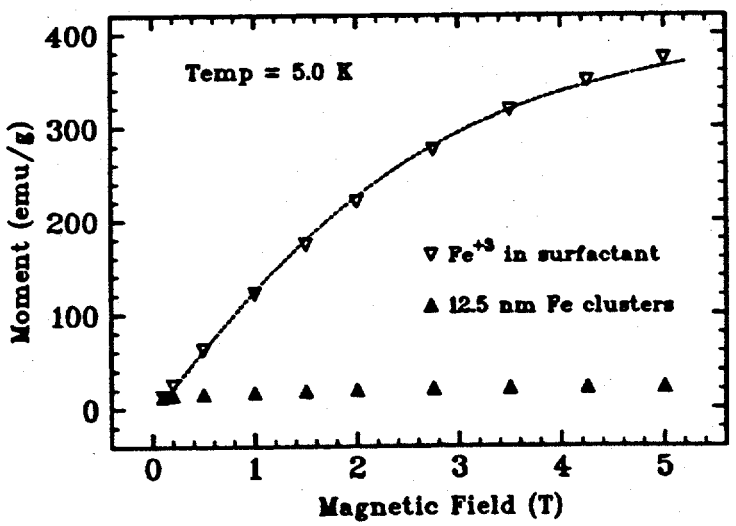

Figure 20. Magnetic moment vs applied magnetic field at 5 °K for 12.5 nm Fe clusters coplotted with the response of Fe^{+3} ions in the precursor solution.

Fig. 21 shows isothermal hysteresis data (moment M versus applied magnetic field H) measured at 5 K following zero-field cooling. The open circles denote the initial response to an increasing field, the solid triangles for a decreasing field, and the open

triangles for an increasing field. The data are shown between -0.25 and +0.25 tesla, but the actual hysteresis measurement used field strengths to ± 2 tesla. These 12.5 nm α-Fe clusters are ferromagnetic at 5 K with the data approaching saturation and exhibiting reversibility at high field strengths. There is a substantial remanent moment M_{rem} at zero field and a moderate coercive field H_{Coer} (where the moment crosses through zero following saturation). The saturation moment for these particles at 5 K, determined by plotting M versus 1/H and extrapolating to infinite field, is 2.2×10^{-3} emu or ~25 emu/g for the 88 μg of Fe in this sample; the saturation moment for bulk α-Fe is 220 emu/g at low temperatures[24]. The total diamagnetic (negative) signal from the surfactant, solvent, glass NMR tube and reducing agent salts (measured in a separate experiment) is linear in applied field and -6.8×10^4 emu in 1 tesla at 5 K; all data have been corrected for this diamagnetism. Although this correction is small at the fields strengths in Fig. 21, it is large at 5 tesla for the dilute Fe samples studied here. Since the Fe sample plus surfactant/solvent/reducing agent is measured independently from the diamagnetic correction, there is considerable uncertainty in the determination of a saturation value by plotting the corrected moment versus 1/H due to the dominance of the correction term.

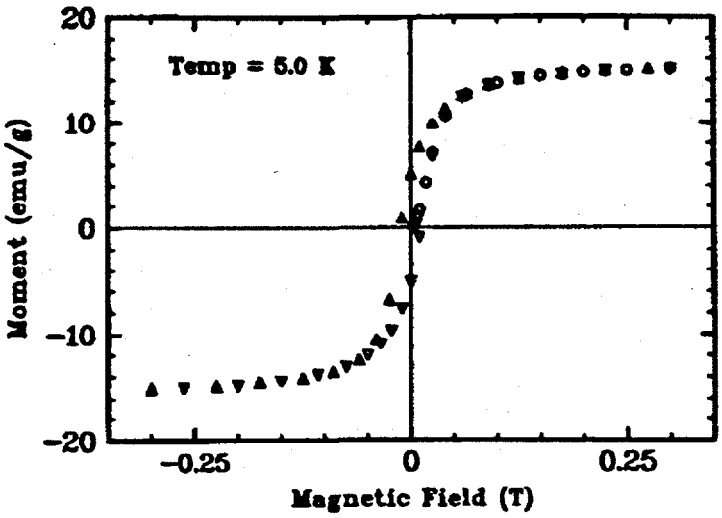

Figure 21. Isothermal hysteresis data (moment M versus applied magnetic field H) measured at 5 K following zero-field cooling for the 12.5 nm α-Fe clusters. The open circles denote the initial response to an increasing field, the solid triangles for a decreasing field, and the open triangles for an increasing field.

The magnetic moment of each Fe particle in a frozen solution will exhibit random rotations driven by thermal fluctuations.[25] Opposing these fluctuations is the magnetic anisotropy energy $E_{aniso} = KV$ where K is the anisotropy energy per unit volume and V

is the volume of the particle. An assembly of such particles will relax to equilibrium through thermal fluctuations on a time scale τ given by

$$\tau = \tau_0 \exp[KV/kT] \qquad (1)$$

where τ_0 is a characteristic time on the order of 10^{-9} seconds, k is the Boltzmann constant and T the absolute temperature.[26]

One of the distinguishing features of small, single domain magnetic particles is the appearance of a blocking temperature T_B defined as the temperature where the relaxation time τ in Eq. (1) becomes comparable to the experimental time of 100 seconds. For temperatures above T_B, the magnetization versus applied magnetic field is reversible due to thermal fluctuations, i.e., the sample exhibits no remanence or coercivity in a hysteresis measurement.[26] α-Fe has cubic anisotropy with an anisotropy energy K_{Fe} of 4.6×10^5 ergs/cm^3; the easy direction for magnetization is one of the [100] axes. For spherical Fe particles with cubic anisotropy, the K in Eq. (1) must be replaced by K/4.[26] Using Eq. (1) for the 12.5 nm Fe particles and $\tau_0 = 10^{-9}$ seconds, we predict $T_B \sim 34$ K for a thermal relaxation time of 100 seconds (the calculated relaxation time is 3×10^{-9} sec at 20 K and 18 nsec at room temperature).

An experimental blocking temperature can be determined from isothermal hysteresis measurements using the vanishing of remanence and coercivity. Fig. 22 shows the remanent moment and coercivity versus temperature for the 12.5 nm particles; both vanish between 50 and 60 K. This experimental T_B is only 50% higher than the calculated value and the latter is extremely sensitive to particle size and morphology. For example, 14 nm particles have a predicted T_B of 47 K which would agree with our experimental result. In addition, various improvements to Eq. (1) have been suggested.[27] We have also studied a sample with 3.7 nm α-Fe particles and found an experimental T_B of 15 K. The volume of these particles is only 2.6% of that for the 12.5 nm clusters, and Eq. (1) predicts a blocking temperature of 0.9 K. The cause of this large disagreement between simple theory and experiment for these 3.7 nm clusters is not understood. It may be that the assumptions of spherical particles and bulk magnetic anisotropy are not valid for very small cluster sizes.

The magnetic results for the saturation magnetization, M_{sat}, remanent moment, M_{rem}, coercivity, H_{coer}, and superparamagnetic blocking temperature, T_B, of our 12.5 ± 0.5 nm α-Fe clusters differ considerably from literature values, M_{sat} is ~25 emu/g at 5 K from extrapolation of magnetization versus 1/H or roughly 10% of the 220 emu/g for bulk α-Fe. Literature values range from 20% of bulk Fe for ~10 nm particles [19-22]

to the bulk value for Fe clusters with 500 to 700 atoms [28] (~2.5 nm diameter). However, the 10 nm particles were oxidized [19,22] and the effects of an oxide shell on the measured M_{sat} of the α-Fe core are not clear. M_{rem} is ~5 emu/g at 5 K and vanishes between 50 and 60 K for the 12.5 nm Fe clusters in inverse micelles compared to 30 emu/g at both 220 and 300 K for oxidized Fe particles with a 3.3 nm diameter metallic core{19]. Again, oxidation of the Fe clusters appears to drastically alter the superparamagnetic transition and remanence.

Coercivity varies strongly with particle size, reaching a maximum for ~15 nm particles of Fe and Co.[29] However, the origin of the coercivity is poorly understood, particularly the effect of surface oxide. The maximum calculated H_{coer} for single domain Fe particles is 50 mT due to magnetic anisotropy while measured values are twice as large.[29] Oxidized α-Fe can have H_{coer} up to 340 mT at 10 K for 6 nm particles [19] and 160 mT for 13 nm particles [20]. The latter is a factor of 20 larger than H_{coer} ~ 8 mT at 10 K for the 12.5 nm α-Fe particles studied here (Fig. 22). More importantly, oxidized Fe particles with α-Fe core diameters between 8.4 and 14 nm exhibited strong coercivities of 40 to 110 mT at room temperature [19], while the coercivity of our 12.5 nm α-Fe particles decreases rapidly with increasing temperature and vanishes between 50 and 60 K, i.e., at T_B (Fig. 22). In one experiment, Fe particles between 6 and 22.7 nm in diameter were synthesized by gas evaporation, collected on a Ag film and covered by a second Ag film inside the evaporation chamber to minimize oxidation.[197] These samples exhibited large, nearly temperature-independent H_{coer} [19], strikingly different from the behavior of the present Fe clusters.

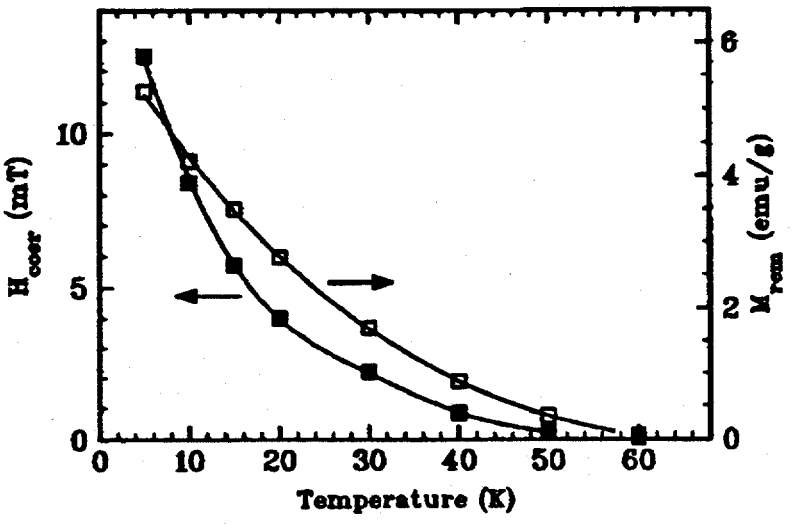

Fig. 22. Coercive field and remanent moment versus temperature for 12.5 nm α-Fe clusters.

In summary, superparamagnetic blocking temperatures were 50-60 K for 12.5 nm clusters and 15 K for 3.7 nm clusters in inverse micelles. The former value agrees reasonably well with the calculated T_B based on cluster size and the magnetic anisotropy of bulk Fe while the latter value is considerably above the calculated T_B. Reported values ranged from 230 K for 5.3 nm Fe cores to 120 K for 2.5 nm cores of oxidized clusters.[19] Granular films with 3 to 9 nm α-Fe particles in a BN host matrix had a field-dependent blocking temperature between 35 and 40 K.[21] However, particle interactions were evident in the strong dependence of coercivity on Fe concentration [21] and these interactions may affect the measured T_B.

The magnetic properties of our monodisperse, isolated and oxide-free α-Fe nanoclusters are very different from those reported in the literature and prepared by other techniques. The earlier work is plagued by oxide layers, poor control over cluster size and generally poor reporoducibility. Although much additional work is needed, we believe that our results may represent the only results on pure α-Fe clusters. Our experiments on clusters in the 1 to 18 nm range provide an opportunity to test various predictions for coercivity, remanence and saturation magnetization as a function of particle size and temperature. The same synthesis has been used for preparing size-selected Co and Ni clusters. The magnetic behavior of these particles should identify the separate roles of thermal energy, magnetic anisotropy and surface versus "bulk" atoms as the cluster size approaches a few unit cells, thus improving our understanding of magnetic phenomena in this size range.

C. Control of Nanocrystal Structure

The equilibrium crystal structure of a material may not always be achieved when nanocrystal growth occurs in an inverse micelle system. We note that such growth occurs at room temperatures where atoms might become trapped at non-equilibrium sites during the growth process. Though there have been reports of amorphous nanosize materials including iron formed by various synthetic approaches, our inverse micellar process invariably leads to the formation of highly crystalline nanophase materials. In this work we have discovered a method for forming both the equilibrium α-Fe phase which has a bcc structure as well as the high temperature γ-Fe phase which has a fcc structure. Since the micelle synthesis process takes place at room temperature the observation of fcc structure in the first iron samples we synthesized was very surprising.

In figure 23 we show a high resolution TEM lattice fringe image of several Fe nanoclusters formed in a cationic surfactant. All of our initial samples were made in this surfactant and all of the clusters with sizes less than 6-8 nm had the γ-Fe structure. This rules out a cluster size-dependent explanation for this unexpected lattice symmetry in the 2.5-6 nm range. The lattice spacing obtained from this TEM was shown to be consistent not with α but γ iron. Cationic surfactants are known to be very strongly binding surfactants compared to nonionic ones and can be shown to easily displace them on the cluster surface.

Selected area electron diffraction (SAD) from these samples confirmed this result, and figure 24 shows the diffraction rings from the 6 nm size iron nanoclusters of figure 23.

Later in this program it was desired to use an uncharged nonionic surfactant to grow iron clusters for use in magnetic studies. When these clusters, which could be size controlled between 2.5 and 15 nm, were examined by SAD, we observed the diffraction pattern shown in figure 25. The symmetry of this pattern is clearly different to even a diffraction neophyte and, in fact, perfectly matches the spacing expected for α-Fe.

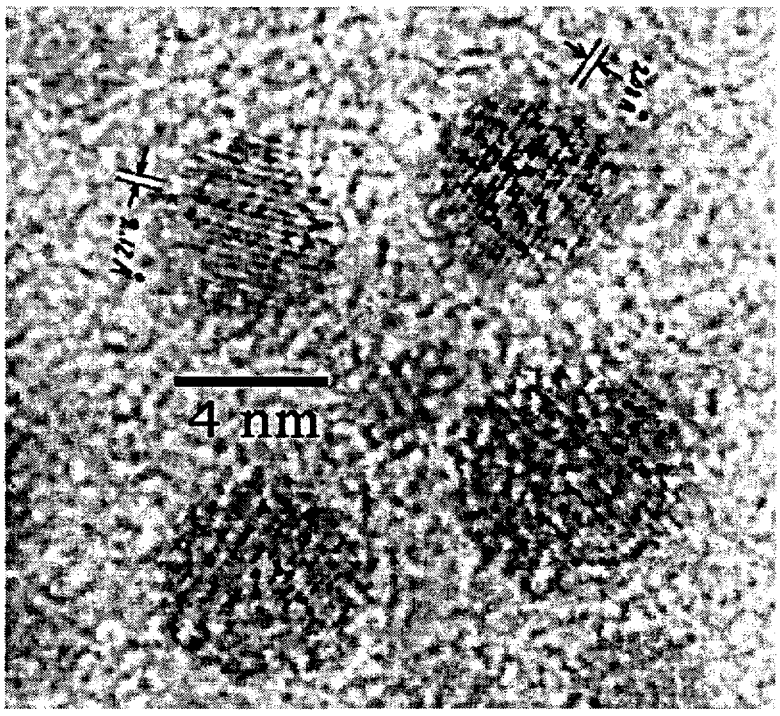

Figure 23. Lattice fringe image of 6 nm size γ-Fe clusters. The lattice spacing of 2.12 Å is shown. The clusters were grown in a cationic surfactant system.

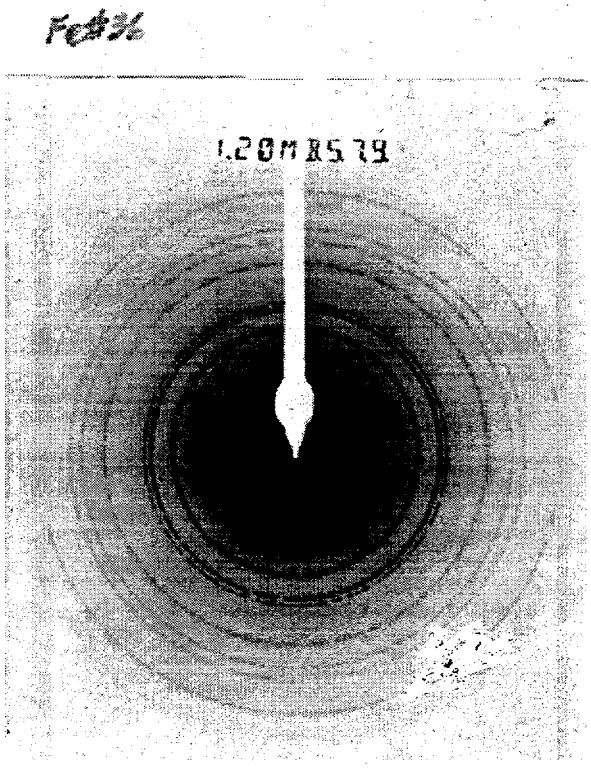

Figure 24. Selected Area electron diffraction from a field of 6 nm size iron clusters grown using a cationic surfactant shows fcc symmetry and lattice spacing consistent with the high temperature γ-Fe phase.

A reasonable inference from these studies is that for nanosize iron the energy difference between the possible cubic structures in the nanoclusters is quite small and that, during the growth process small differences in the preferential binding site of the surfactant used alter the final crystalline phase of the iron. An additional factor is that the type of solvent used in the synthesis itself may influence the final structure by interacting with the growing surface of the cluster. Evidence for this comes from growth studies in coordinating solvents such as toluene or tetrahydrofuran in which the non-equilibrium γ phase is often observed. Thus, a complete understanding of the best methods of phase control requires further research.

It is also possible that the phase diagram for nanosize iron is different from that of the bulk such that the phase boundary between γ and α-Fe occurs at a significantly depressed temperature relative to the bulk. It has been fairly well established that liquid-solid phase boundaries (melting temperatures) in nanosize materials are significantly depressed compared to the bulk, so it would not be strange to observe changes in structural phase transition temperatures as well. It fact, our observations with iron

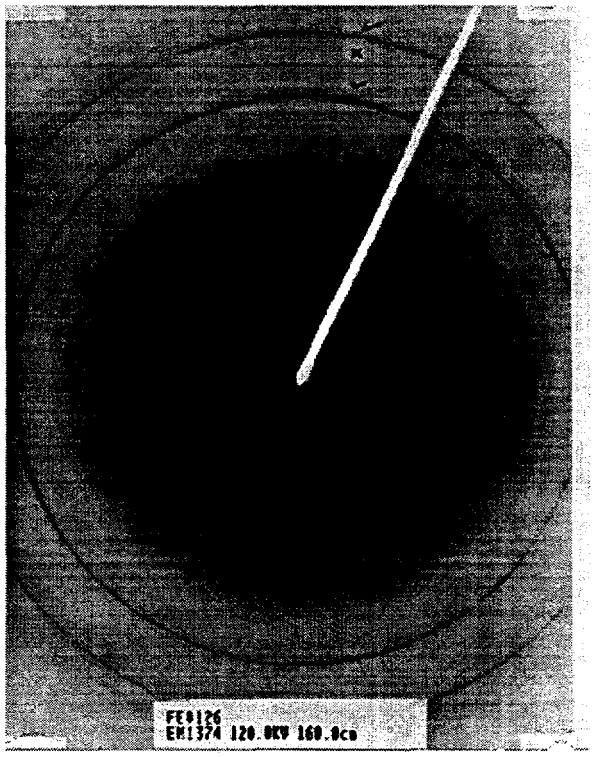

Figure 25. Selected area electron diffraction from a field of 4.3 nm iron clusters grown in a non-ionic inverse micelle system. The symmetry matches of the bcc pattern of α-Fe.

nanostructure are a strong motivation to examine other well-known phase transitions such as α to β Sn which occurs at -13.2°C in the bulk. Important issues are: does the transition still occur in nanosize materials and what is its size dependence? We have initiated some preliminary studies of tin nanoclusters to address these issues.

V. Dielectric Properties of Nanoclusters

A. The Dielectric Constants of Metallic Clusters

The dielectric constants of a substance are among its most fundamental properties. Both applied and fundamental scientific considerations motivate the strong interest in the dielectric constants of nanoclusters. On the applied side, knowledge of these constants is important in such applications as catalysis, photocatalysis, microcapacitors, microelectronics and nonlinear optics. From the fundamental point of view, the possible influences of cluster size and of the discretization of the energy level structure at small cluster sizes on the dielectric properties have been subjects of much theoretical and some experimental interest. The early interest was stimulated by a much-referenced paper by Gor'kov and Eliashberg[31] which took into consideration the influence of quantum effects on the properties of metallic nanoclusters. One of the main results of this work was the prediction of a quantum size-related dramatic enhancement ($> 10^2$ x) of the electric polarizability of these clusters at low frequencies compared to large clusters or bulk. Definitive experimental verification of this result proved difficult because of the major difficulty of producing desired samples, namely ones which contain sufficiently high concentration of monodisperse clusters of known size. The relatively few early experimental attempts failed to confirm the prediction, and subsequent theoretical work refuted it due to improper treatment of depolarization effects in Gor'kov and Eliashberg's work.[32]

Although it is now generally acknowledged that the "dramatic enhancement" effect of Gor'kov and Eliashberg may not exist, there is still much theoretical debate as to whether the electric polarizability is enhanced or depressed relative to its classical (large size) value for small nanoclusters.[32] Additionally, there have been relatively recent reports of large positive dielectric constants for metal clusters in the sub-micron size range.[33] This is a rather unusual result since the dielectric constant of metals is negative as a consequence of the dominating inductive free carrier contribution to the polarization.

In principle our synthesis approach, based on the use of inverse micellar cages as reaction vessels, is ideal for producing the size-selected nanocluster samples needed to shed some light on the possible influence of quantum confinement on the polarizabilities of metal and semiconductor nano-clusters. We are also quite interested in the confirmation of Nimtz and Marquardt's finding of very large positive dielectric constants

for metal nanoclusters.[33] If true, this is a very significant finding that has strong technological implications for two areas which motivate our own work on nanoclusters, namely microdevices and catalysis.

We have demonstrated greatly enhanced catalytic activity for both metal and semiconductor nanoclusters,[34] but the origin of this effect is not well established. The implication of a large positive dielectric constant of a cluster for catalysis relates to the possible inherent shielding of the repulsive electric forces between reactants brought about by such a cluster.[33] This effect can be seen as follows. The Coulomb repulsive force F between charges q_1 and q_2 a distant r apart is to a good approximation

$$F = q_1 q_2 / \epsilon_0 \epsilon_1 \pi r^2, \tag{2}$$

where ϵ_0 is the permitivity of free space and ϵ_1 is the real part of the dielectric constant. A large positive ϵ_1 of a catalyst can strongly increase the effective ϵ_1 of the medium about it and thereby reduce the long-range repulsive forces of the reactants. This shielding effect in principle would allow reactants to come closer together and react in the vicinity of the cluster catalyst. An assessment of this effect is clearly important, for it could provide a significant key to the origin of catalytic activity of clusters and, more generally, metals.

In the present work we have synthesized several metallic and semiconductor nanoclusters in solution, built a cell suitable for measuring the dielectric constants of solutions and begun to study the dielectric properties. Before presenting some of our results, it is necessary to provide a brief theoretical background needed for understanding these results.

B. Theoretical Considerations

The generic problem of interest is that of polarizable metallic clusters (for now assumed spherical) of dielectric constant ϵ embedded in a dielectric medium of dielectric constant ϵ_m. At issue is the relationship of the effective dielectric constant of the medium plus clusters, ϵ_{eff}, to ϵ_m and ϵ. The presence of the clusters gives an extra contribution to the effective dielectric constant of the medium. Charge accumulation at the cluster-medium interface produces a depolarizing field which causes the field inside the cluster, E_{loc}, to be lower than the externally applied field, E_0. The relationship between these two fields can be expressed as

$$E_{loc} = E_0 - 4\pi DP, \tag{3}$$

where D is the depolarizing factor and P is the polarization, which is the dipole moment per unit volume, m, induced on the cluster. For the present case it is easily shown that [34]

$$\mu = \frac{\pi d^3}{6}\left(\frac{\epsilon - \epsilon_m}{\epsilon + 2\epsilon_m}\right) 3\epsilon_0 E_0. \tag{4}$$

The plasmon resonance of the metallic cluster is given by the frequency ω_R for which $\mu \to \infty$, i.e., for $\epsilon(\omega_R) + 2\epsilon_m = 0$.

The induced polarization P is related to E_0 through the polarizability, α, by

$$P = \alpha E_0, \tag{5}$$

and to E_{loc} through the electric susceptibility, χ, by

$$P = \chi E_{loc}. \tag{6}$$

Combining Eqs. 3, 5 and 6 yields

$$\alpha = \chi V / (1 + 4\pi D\chi) \tag{7}$$

which can be determined from low-frequency capacitance measurements of the static dielectric constant $\epsilon_{(0)}$ through[32]

$$\epsilon_{(0)} = \epsilon_m \left[\frac{1 + \frac{2}{3} f(\alpha / V)}{1 - \frac{1}{3} f(\alpha / V)}\right], \tag{8}$$

where f is the volume fraction of metal. Considering the cluster to be a small metal sphere, its classical polarizability, i.e., its α in the absence of quantum effects, is $\alpha = 3V$, a well-known result.[32] For small filling fraction ($f \ll 1$) Eq. 8 then reduces to

$$\epsilon_{(0)} / \epsilon_m = 1 + 3f \tag{9}$$

for the ratio of the dielectric constant of the metal cluster-in-a-medium relative to that of the medium. Thus, in the classical limit and for small concentration of clusters the enhancement of ε is very modest and simply proportional to f.

The outstanding issue relative to the role of quantum size effects in determining the dielectric response is whether or not these effects enhance α over that of its classical limit. Representing such enhancement by the parameter A, α in the quantum limit becomes $\alpha = 3AV$, and Eq. (9) becomes

$$\epsilon_{(0)} / \epsilon_m = 1 + 3Af. \tag{10}$$

In the context of Gor'kov and Eliashberg's results,[39] A is very large ($>10^2$). Under favorable conditions Eqs. 9 and 10 can be tested directly by dielectric measurements.

The relationship between ϵ_{eff} and ϵ_m and ϵ can be easily derived in the classical limit.[34] For an isotropic spherical particle the Lorenz local field factor is $4\pi/3$ which leads to

$$E_{loc} = \frac{1}{3}(\epsilon_{eff} + 2\epsilon_m)E_0. \tag{11}$$

This form of E_{loc} leads to the well known Maxwell Garnett equation.[34]

$$\left(\frac{\epsilon_{eff} - \epsilon_m}{\epsilon_{eff} + 2\epsilon_m}\right) = f\left(\frac{\epsilon - \epsilon_m}{\epsilon + 2\epsilon_m}\right) \tag{12a}$$

Equation (12a) is often written in the form

$$\epsilon_{eff} = \epsilon_m \left[\frac{1 + 2f(\epsilon - \epsilon_m)/(\epsilon + 2\epsilon_m)}{1 - f(\epsilon - \epsilon_m)/(\epsilon + 2\epsilon_m)}\right]. \tag{12b}$$

Thus, by measuring ϵ_{eff} and ϵ_m and knowing f we can calculate the dielectric constant of the clusters. Equation (12) has been very successful in explaining the dielectric and optical properties of submicroscopic dispersions of metals.[35] It is applicable in the dilute limit ($f<<1$) and for cluster diameters smaller than the wavelength of the radiation inside the medium.

Finally, we note that the dielectric constant is a complex quantity, i.e.,

$$\epsilon = \epsilon_1 - i\epsilon_2, \tag{13}$$

where ϵ_1 and ϵ_2 are the real and imaginary parts, respectively. For metallic and elemental semiconductor (e.g. Si, Ge) clusters the only source of polarization is electronic and $\epsilon \equiv \tilde{n}^2$, where $\tilde{n}$ is the complex refractive index which can be written as

$$\tilde{n} = n - i\kappa, \qquad (14)$$

where n is the real part of the refractive index and κ is the extinction coefficient which measures the attenuation of the wave in the medium. From Eqs. 13 and 14 it is readily seen that $\epsilon_1 = n^2 - \kappa^2$ and $\epsilon_2 = 2n\kappa$. The case of partially ionic semiconducting clusters is more complex. Here there are two sources of polarization, electronic and lattice, the latter having to do with the polarization induced by the opposite displacements of positive and negative ions in response to an applied electric field.

C. Results and Discussion: Pd and Au Clusters

We have performed measurements of the complex dielectric response on Pd and Au clusters dispersed in various media and initiated some preliminary studies on CdS and MoS_2 clusters. Essentially all of these measurements were carried out at room temperature (~ 295K) and covered the frequency range 10^2 - 10^6 Hz. The most extensive measurements were on Pd clusters, and we summarize these results first.

Five Pd cluster samples (#s 76, 78-81) were grown in the hydrocarbon decane (c10) using the nonionic surfactant Brij 30, and three other samples (#s 75, 82 and 83) were grown in octane (c8) with the anionic surfactant AOT. These syntheses produced Pd clusters in the size range 1.6 to ~ 10 nm, with the TEM sizes shown in the Table below

Table I. TEM size of Pd Clusters

sample #	75	76	78	79	80	81	82	83
diameter(nm)	10	2.6	2.8	2.8	1.6	4.2	2.3	2.3

Results on the first five samples were identical as were the results on the second set of three samples. The results on the two sets were also essentially identical above 10^4 Hz, but differed somewhat at lower frequencies, the first set of five yielding larger values of ϵ_1.

Before presenting some of the results we note that although our synthesis method produces excellent monodisperse clusters, interpretation of the dielectric data is at present complicated by a number of factors. First, our clusters are embedded in a complex medium which consists of the solvent (decane or octane) plus surfactant. Secondly, the clusters are encapsulated in a surfactant cage. Thirdly, the potential exists for some residual ionic species which are byproducts of the synthesis to remain in the solution and

influence the dielectric response. In the future these complications will be overcome by the use of the chromatographic separation technique developed in this program to remove residual species and by the removal of the surfactant capping layer. In the meantime, however, the dielectric constants reported below should be viewed as effective values for the capped clusters.

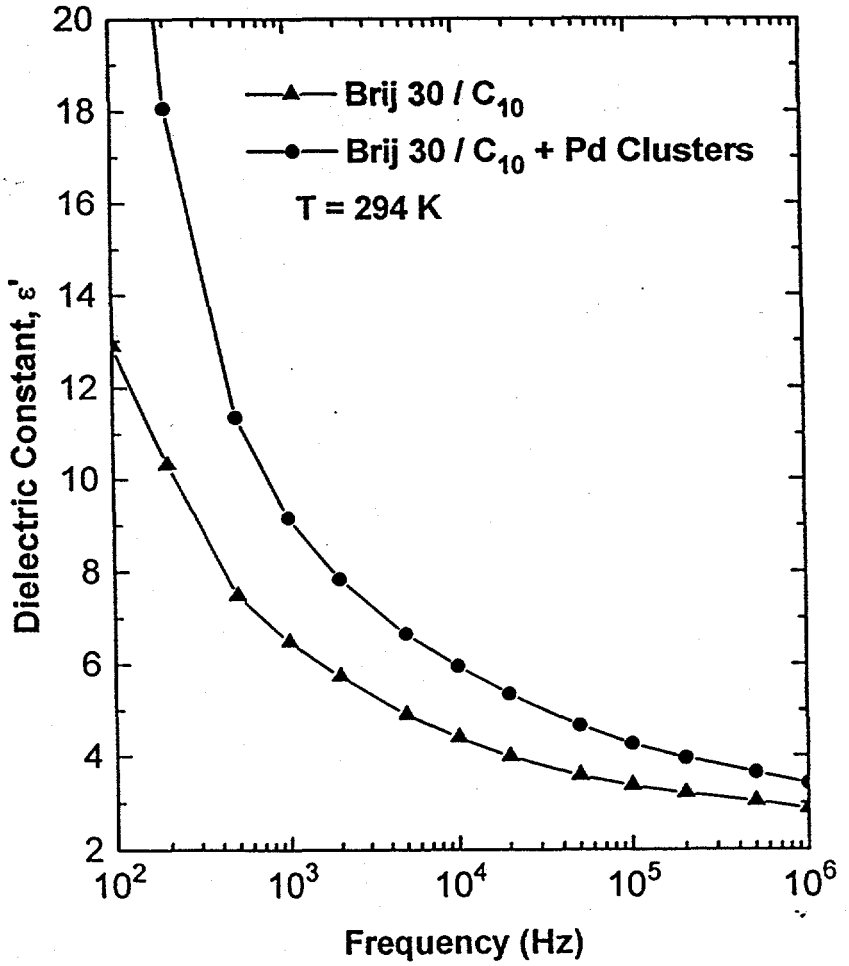

Figure 26. Real part of the dielectric constant vs frequency for Brij 30/c10 precursor micellar system (lower curve) and same micellar system containing Pd #78 clusters (2.8 nm diameter) where the volume fraction of cluster is $f \sim 10^{-4}$.

Figure 26 shows typical behavior of the real part of the dielectric constant as a function of the frequency of the applied field. The lower curve shows the response of the decane plus surfactant whereas the top curve represents the behavior of the solution plus clusters. Several features in the data can be noted. Both responses exhibit large decreases of ϵ_1 with increasing frequency and appear to be approaching asymptotic values at $\sim 10^6$ Hz. This large frequency dispersion and the large values of ϵ_1 at low frequencies are suggestive of large ionic conductivities in both cases, a feature that is

confirmed by the large and strongly frequency-dependent dielectric losses (or tan δ; tan δ is related to by $= \epsilon_1 \tan \delta$) for the same samples shown in Fig. 27. As can be seen, tan δ for samples with and without clusters decreases rapidly with increasing frequency and approach low values characteristic of normal dielectrics at ~ 10^6 Hz. The decreases in both ϵ_1 and tan δ with increasing frequency reflect the increasing inability of ionic species to follow the electric field. At sufficiently high frequencies these species are frozen out and do not contribute to the polarization.

For the present purposes the most meaningful data are those at 10^6 Hz, i.e. close to the asymptotic limit. Figure 26 clearly shows enhancement of ϵ_1 due to the presence of the Pd clusters (plus possibly some residual ionic species), and we take the difference between the two curves at 10^6 Hz $(\Delta \epsilon_1 = 0.64)$ to represent the upper limit of the contribution of the clusters.

At 10^6 Hz the data in Fig. 26 yield ϵ_1 ($\equiv \epsilon_{1,eff}$, i.e., ϵ_1 of the solution plus clusters) = 3.48 and $\epsilon_{1,m}$ = 2.84. Given that the volume fraction (f) of clusters in the sample of Fig. 26 is ~10^{-4}, Eq. (10) with $\epsilon_1 / \epsilon_{1m} = 1.23$ suggests that the enhancement factor A~ 770.

The fact that this value is close to that predicted by Gor'kov and Eliashberg must be viewed as fortuitous, since, as already cautioned, the above values of ϵ' and ϵ'_m may be influenced by the capping layer and by the presence of ionic species. The final resolution of this issue must await the purification of the samples.

Using Eq. 12, the above values of $\epsilon_{1,eff}$, $\epsilon_{1,m}$ and f ($\approx 10^{-4}$) yields ϵ_1 = -5.7 as the dielectric constant of the "capped Pd clusters." Note that ϵ_1 is negative.

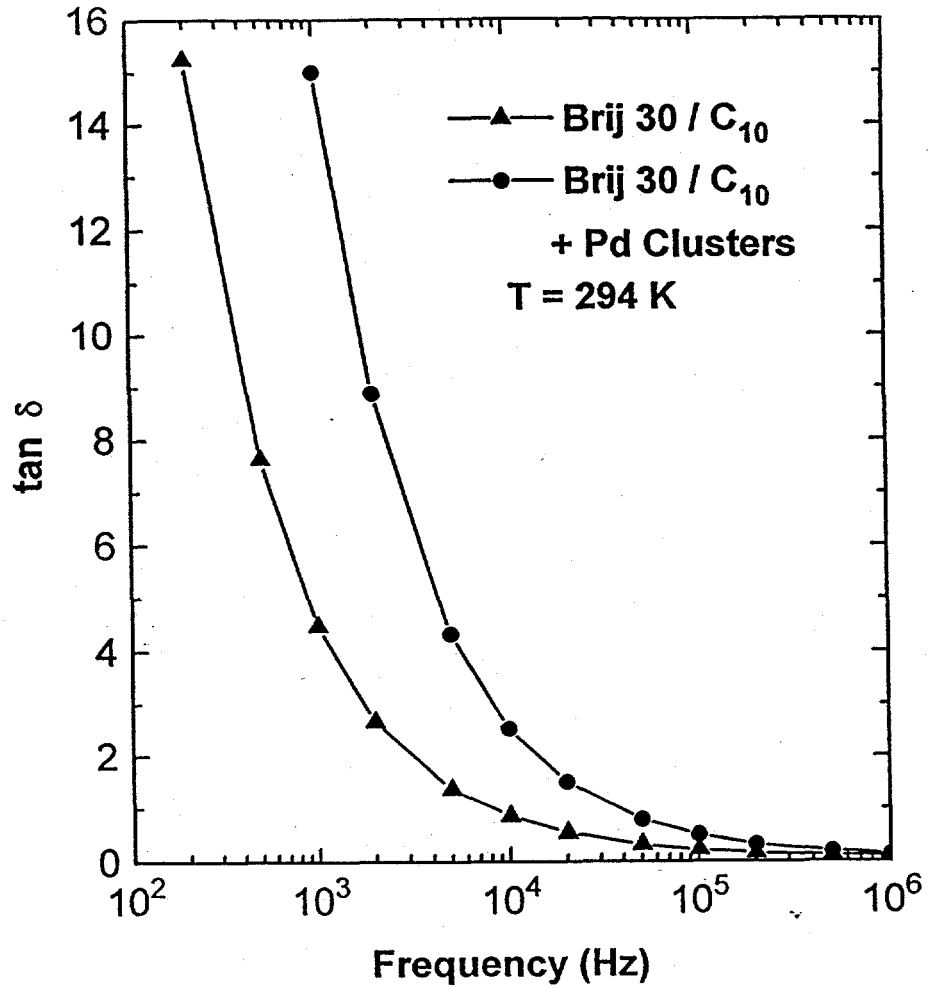

Figure 27. Loss tangent, tan δ, vs frequency for Brij 30/c10 precursor micellar system (lower curve) and same micelles containing Pd #78 clusters (2.8 nm diameter) where $f \sim 10^{-4}$.

Turning next to nm diameter gold (Au) clusters, two sets of samples were investigated. The first set consisted of 4.0 nm Au clusters grown in micellar cages in octane at a volume fraction of 1×10^{-4}. The results were very similar to those for Pd clusters in decane (Figs. 26 and 27), and the ϵ_1 values at the high frequency end yielded $\epsilon_1 = -4.2$ for the "clusters." Again we note the negative value of ϵ_1.

The second set of Au samples were grown in solution (styrene and surfactant) and subsequently embedded in polystyrene. These 8.3 nm clusters were made into a solid plastic by adding cross-linking agent (divinylbenzene) and initiator, AIBN, and cross-linked in situ at 60 °C. The resultant material was a solid which was light purple in color. A second sample which did not contain clusters was prepared in the same way resulting in a milky colored solid. Thin disks were cut from both samples, polished and electroded with Ag paste. Figures 28 and 29 show ϵ_1 and tan δ, respectively as

functions of frequency. The responses are qualitatively similar to those of Au and Pd in solution, but the dielectric losses are considerably smaller. In particular, without the clusters, the polystyrene behaved as a good dielectric; however, the sample with the clusters appears to contain some trapped polarizable ionic species. Its ϵ_1 appears to be approaching an asymptotic value above ~ 10^5 Hz. At this frequency $\epsilon'_{1,eff}$ = 3.73 and $\epsilon_{1,m}$ = 3.56 yielding $\epsilon_{1,eff} / \epsilon_{1,m}$ = 1.05, which for the low cluster concentration used (f ~ 10^{-4}) suggests an enhancement factor A~170 which is again large. These values of ϵ_1 yield via Eq. 12 ϵ_1 = -7.2 for the effective real part of the dielectric constant of the Au clusters in the polystyrene matrix. This value of ϵ_1 is comparable to those of both the Pd and Au clusters in solution.

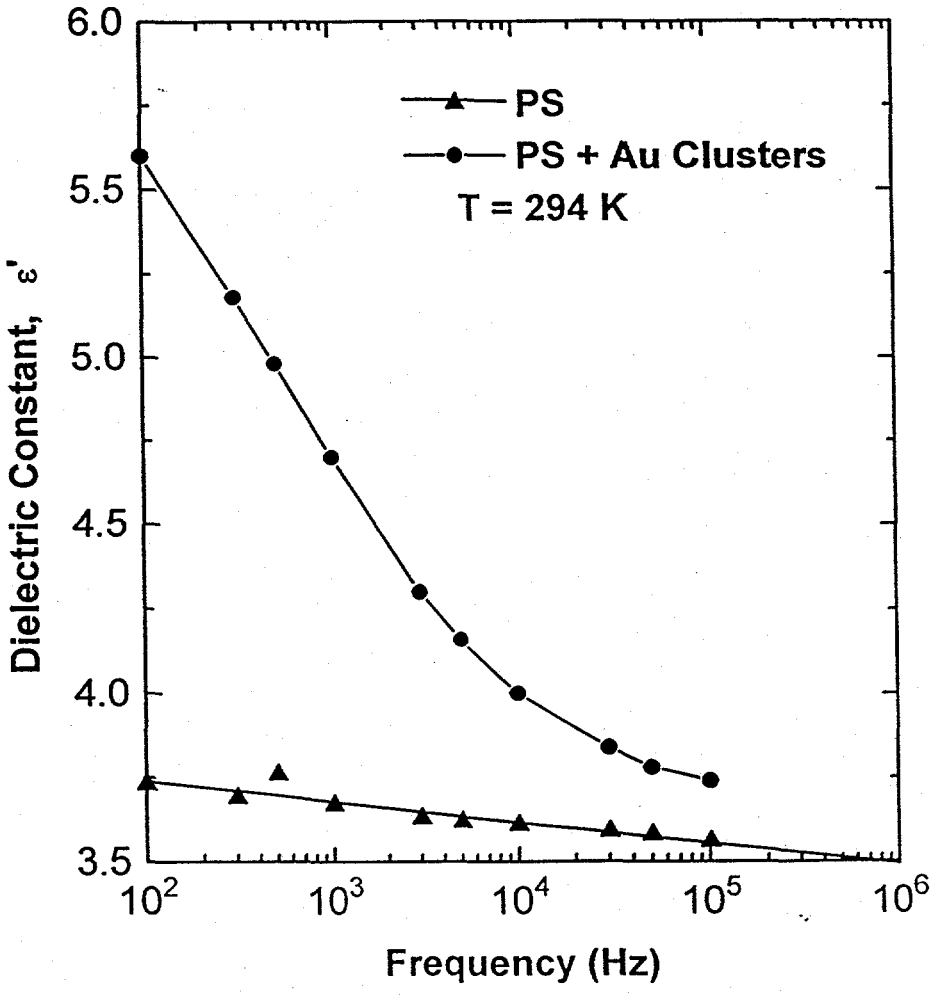

Figure 28. Real part of the dielectric constant vs frequency for 8.3 nm diameter gold clusters encapsulated in cross-linked polystyrene is compared to the polystyrene matrix itself (lower curve).

The negative sign of the effective ϵ_1 for the Pd and Au clusters deduced from our data is the expected result for metals. Thus, we do not see any evidence for positive ϵ_1's as reported by Nimtz and Marquardt[33]. However, it should be noted that the several metallic clusters investigated by these authors were considerably larger (50 - 10^4 nm) than our own (< 10 nm) and their concentration (f = 0.1) was also much larger than ours ($f \sim 10^{-4}$). Thus, the issue of positive ϵ_1 for large metallic clusters, though puzzling, remains open.

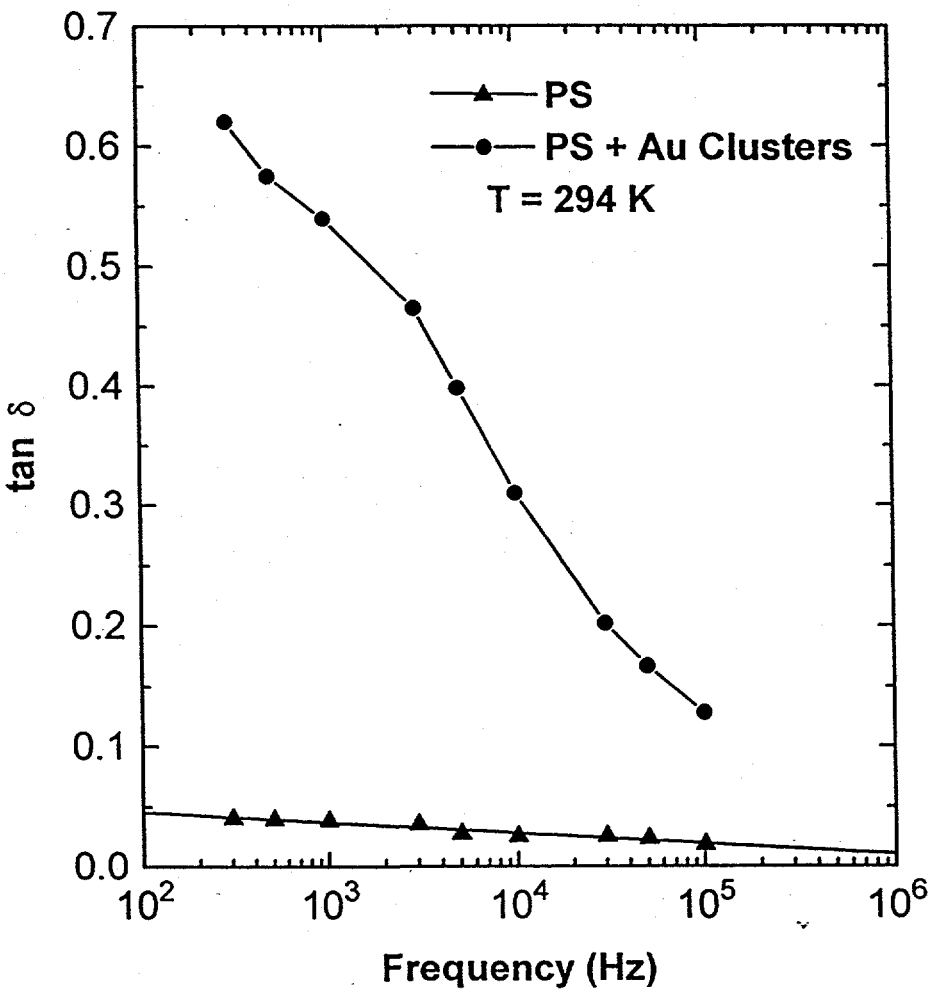

Figure 29. Loss tangent tan δ vs frequency for 8.3 nm diameter gold clusters encapsulated in cross-linked polystyrene is compared to the polystyrene matrix itself (lower curve).

Ashrit et al[36] recently studied the optical reflection and transmission properties of 10 and 22 nm silver (Ag) clusters dispersed in gelatin films. Mie theory analysis of their data yielded the real and imaginary parts of ϵ_1 for the clusters. They find negative values of ϵ_1 which increase in magnitude with increasing wavelength. At 800 nm their values are ϵ_1 = -15 and -20 for the 22 and 10 nm clusters, respectively, suggesting that ϵ_1 is

size dependent. However, in view of the fact that there is conflicting evidence in the literature about this point,[37] Ashrit et al's results need confirmation. Despite these uncertainties, it appears that our values of the effective ϵ_1's for the Pd and Au clusters are of the correct sign and order of magnitude.

D. Semiconductor Clusters

Finally, we have made some preliminary measurements on MoS_2 and CdS clusters in solution. These solutions were even more lossy than the Pd cluster solutions, undoubtedly due to the presence of large concentrations of residual ionic species produced in the more complicated synthesis of these compound clusters. More detailed studies are awaiting completion of our chromatographic separation facility. In the case of the MoS_2 clusters, we attempted to carry out the dielectric measurements at low temperatures in order to freeze out the ionic contributions. However, this attempt was complicated by the phase separation of the solvent-surfactant system. By the way, we find that dielectric measurements are a very sensitive probe for studying the phase equilibria of such systems.

VI. Optical Properties of Metallic Clusters

A. Elemental Clusters

The formation of metal colloids by the controlled reduction, nucleation and growth of metal salts in aqueous solution has been investigated for nearly a century. In the case of gold colloids the earliest work dates to Michael Faraday.[38] Much of the interest in gold colloids (or nanoclusters) stems from their remarkable stabilities, monodispersity, and interesting optical properties.

The advantages of forming metal particles which are readily dispersed in organic media is recognized by workers in many fields and their application and properties were discussed in recent review articles.[39,40] For example, in small, particulate, magnetic recording media a thin, well dispersed film containing polymers, metal or metal oxide particles, and lubricants must be deposited on a supporting substrate without particle aggregation ensuing. Another example is in the area of conductive inks where well dispersed gold, silver, or copper particles need to be sprayed onto a polymeric substrate. Such an application requires the use of a low vapor pressure organic solvent which readily wets the surface. In such cases the advantages of colloid preparation in non-aqueous media are obvious. In the present work we were motivated by a desire to tune the optical absorbance properties of small clusters to better match the solar spectrum. In this application the metal particle acts like an antenna to absorb energy which may subsequently be transferred to a semiconductor nanoparticle creating a hole-electron pair. In this regard the metal would function much as dye sensitizers do, but without the chemical degradation and toxicity issues inherent to the use of dyes.

A second scientific motivation for optical studies of metal nanoclusters stems from quantum size theories for metal colloids which predict that the plasmon resonance should broaden considerably as the particle size is decreased. Also, many current ideas[41] suggest that a blue shift in λ_{max} should occur with decreasing size, though the effect should be small. Our observations suggest that, in the size range of 2-5 nm, the effect is surprisingly large as shown in figure 30.

There are conflicting experimental results on the broadening of the plasmon width with decreasing cluster size. For example, experiments on silver sols by Heard and co-workers[42] showed that a four-fold increase in particle size resulted in an increase of 17 nm in λ_{max} but no increase in half-width. Our experiments indicate a significant increase in the half-width in the size range of 8-2 nm and a shift of more than 30 nm in the position of λ_{max}.

Even ignoring these quantum size effects, the optics of dispersed metal clusters or colloids is quite complicated. An accurate description of the optical properties in the simplest case of independent spherical colloids was first developed by Gustav Mie and current ideas were summarized in a recent monograph.[43] Mie's description of the scattering from small metal spheres is so precise as to allow the determination of the complex refractive index of the metal to be calculated as a function of wavelength. Later work[44] showed that such issues as variation of particle size, variation of particle shape, aggregation of the primary particles, and effect of adsorbates (e.g. surfactants) on the surface could affect the observed spectra. Turkevich and coworkers were able to show that as the spherical gold colloid particle size dispersed in aqueous solution increases from 7.5 to 33 nm, the absorption maximum remains at 522 nm for the smallest clusters (7-10 nm), then begins to red shift and broadens with corresponding color changes from purple to violet to blue.[45] At the same time, the extinction coefficient/gram of Au increases with particle size up to a maximum at ~80 nm, and then decreases steadily.

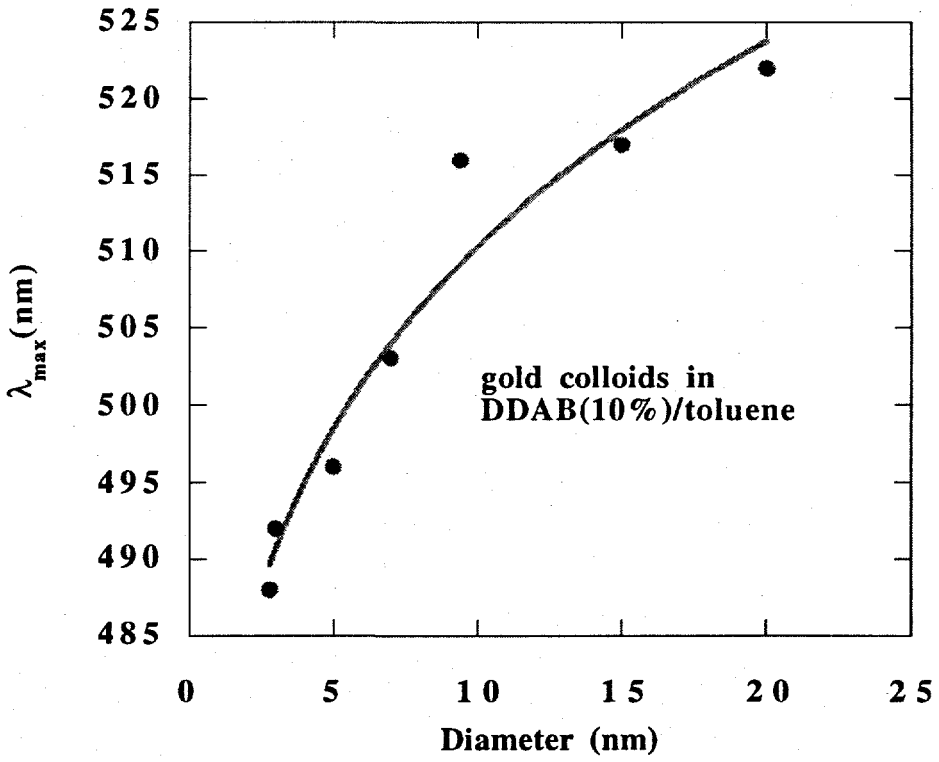

Figure 30. Position of the maximum in the surface plasmon resonance (λ_{max}) vs gold cluster diameter shows significant quantum confinement effects which shift the resonance to the blue.

In our nanoclusters we see more significant shifts in λ_{max}, with very little variation of the extinction, ε, with size, D, in our inverse micellar systems. For example we find λ_{max}~490 nm for D=3.4 nm, λ_{max}=499 nm for D=6.8 nm, and λ_{max}=510 for D=8.3 nm, while the extinction remains roughly constant until D>8 nm. Perhaps these more significant changes in λ_{max} are due to the fact that we are investigating smaller colloids than previous work.

Mie theory, on the other hand, predicts no significant change in extinction in this size range. For example, the extinction should be roughly constant with a value of 7400 cm^{-1}-mol^{-1}, based upon modern values of the optical constants of gold.[46] This value is more than twice the value we observe, suggesting an important role for the surfactant on the cluster surface. If the surfactant donates electron density into the surface, the effective refractive index of the surface will be altered from that of the pure metal, affecting its optical properties.

The theoretical value of the peak extinction is strongly dependent on the measured optical constants used in the calculation. When alternative values are used,[47] the peak extinction is predicted to be ~11,000 cm^{-1}-mol^{-1}, while other values[48] give ε_{max} ~6500 cm^{-1}-mol^{-1} demonstrating the necessity for extreme accuracy in the measurements of the optical constants near resonance if a comparison using Mie theory to experimental extinction measurements is desired. Experimentally, we find the average value of the peak extinction appears to be ~3000 cm^{-1}-mol^{-1} if the system is quite monodisperse and spherical.

The position of the peak absorbance in the classical Mie theory is determined by both the optical constants of the metal and the refractive index, n, of the medium. For example, the classical theory predicts resonances at 500 nm, 520 nm, and 530 nm for particles with sizes less than 20 nm in air (n=1.0) , water (n=1.334), and toluene (n=1.5) respectively. Experimentally, we find the resonance at 520 nm for D=11.3 nm spheres in water, and 512 nm for D=7.3 nm spheres in toluene. The shift is obviously in the wrong direction. However, the latter spheres are stabilized with a surfactant on their surface, which may alter the effective refractive index to be used in the calculation. However, it is perplexing that a wide range of colloids prepared in inverse micelles with various types of nonionic, anionic, and cationic surfactants consistently show a blue, rather than a red shift in resonance compared to their similarly sized counterparts prepared in water. This suggests that there may be other important effects occurring in this small size regime.[23]

B. Composite Clusters

In order to better control the optical properties, it would be desirable to have synthetic methods for altering the surface properties of metal clusters. We have already speculated that the presence of the surfactant may achieve this end to a limited degree. We have now developed a strategy for the synthesis of composite nanoclusters which is rather simple given the basic micellar synthetic method. First, a monodisperse population of clusters (e.g. Au) is grown with a desired size as outlined in reference 23. This cluster population serves as seed particles for the homogeneous nucleation and growth of the other material (e.g. Ag) on its surface.

The optical features of homogenous nanosize populations of Au or Ag clusters are so well known[43] that absorbance measurements alone can determine whether a coated cluster results from this synthetic approach. The other synthetic possibility is the formation of two separate populations of Au and Ag nanoclusters. To rule out this possibility, separate synthesis of Au and Ag nanoclusters solutions were performed followed by simple mixing of these solutions to form a control sample whose optical properties are shown in figure 31.

When sequential reductions are performed to form coated cluster composities the spectra shown in figure 32 result. Interesting features include a significant size dependence for the same atomic composition. Neither spectrum resembles that of the homogeneous solution shown in the figure 31. As expected from theory,[49] direct contact of the two metals alters the optical properties significantly since it changes the refractive index boundary conditions at the cluster surface for the electromagnetic wave which is scattered and absorbed at this surface. For the same reason changes in cluster shape will also alter the optical properties signficantly.

The type of material on the outer surface of the nanocluster has a significant effect on the optical properties as shown in figure 33. The aborption spectra shown in this figure are for 10 nm composite clusters which have the same overall atomic composition. It is worth mentioning that it is unlikely that a uniform coating of either metal on the surface of the nanocluster core is achieved by our process. A highly curved surface of a particle with only a 2-10 nm diameter makes it seem more reasonable to deposit an island-like structure of one material on the other. However, we have not yet been able to resolve this issue by high resolution TEM.

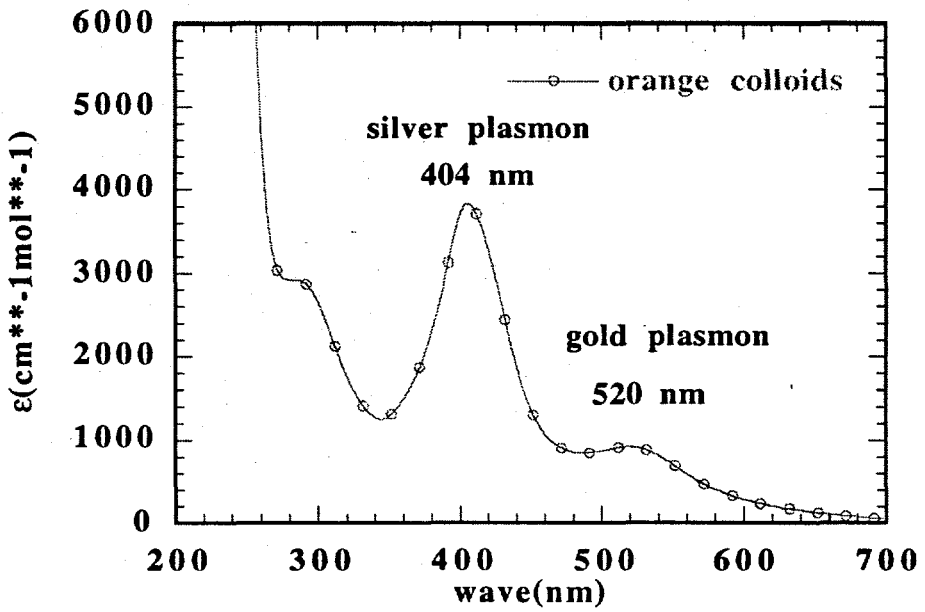

Figure 31. Two homogeneous populations of separately synthesized gold and silver nanoclusters are mixed together. The total spectrum is just the sum of the individual absorbances, and the two plasmons remain in their normal positions as shown, and the solution has an orange color (gold cluster solutions are red while silver ones appear yellow).

In summary, we can tailor the absorbance properties of metal nanoclusters by coating one element on the other. By using varying amounts of one material (e.g. Ag) on another core material (e.g. Au) we can tune the optical absorbance and extinction values over a significant range as shown in figure 34.

This part of our work has an important additional benefit. The ability to selectively coat a cluster with a different material has several technological uses in catalysis and photocatalysis. In catalysis one can imagine coating clusters made from an inexpensive non-catalytically active material (e.g. Fe) with an expensive catalytically active material such as Pt. In photocatalysis the ability to selectively coat semiconductor clusters with metals would be highly significant for controlling optical absorption and carrier recombination properties as well as for the development of novel micro electrochemical cells.

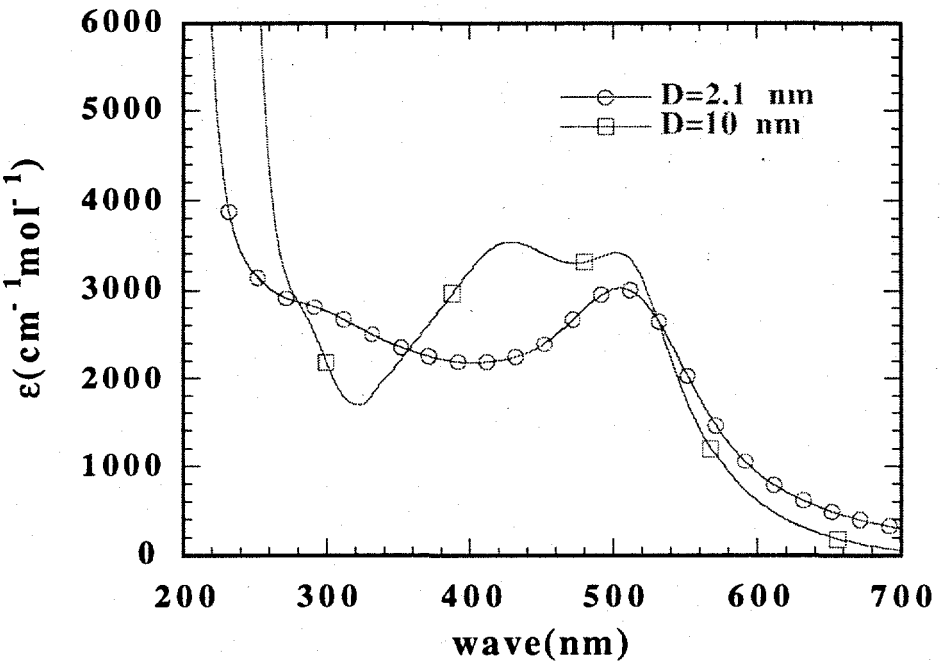

Figure 32. The absorption spectra of 1:1 Au/Ag (core/shell) composite clusters show a significant dependence on cluster size. Neither spectrum resembles that of figure 31 ruling out separate collections of gold and silver nanoclusters.

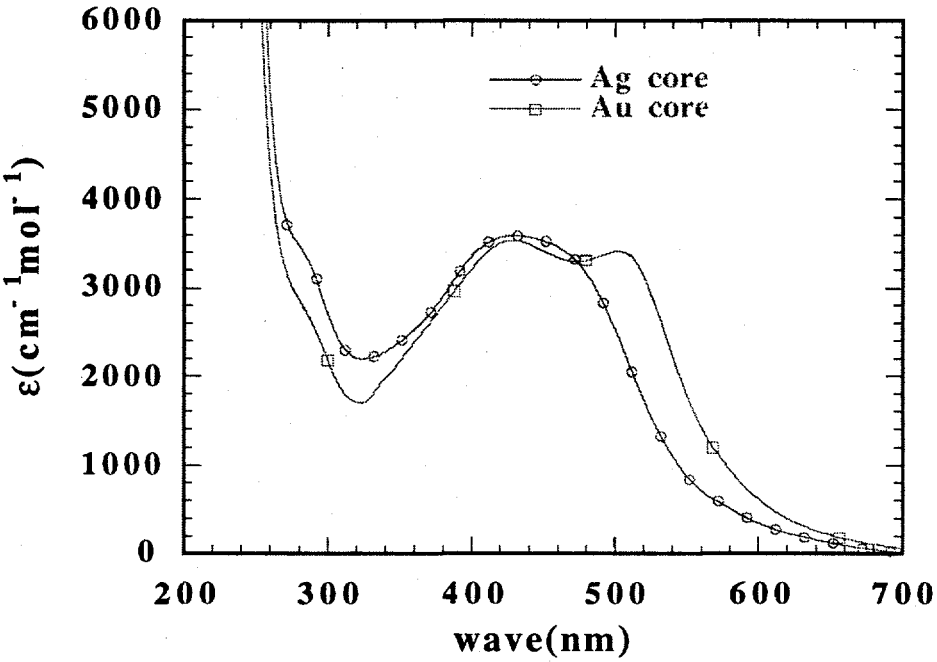

Figure 33. The absorption spectra of 10 nm composite 1:1 Au/Ag and Ag/Au clusters. The metal on the outer surface of the cluster affects the optical properties even for identical atomic composition and size.

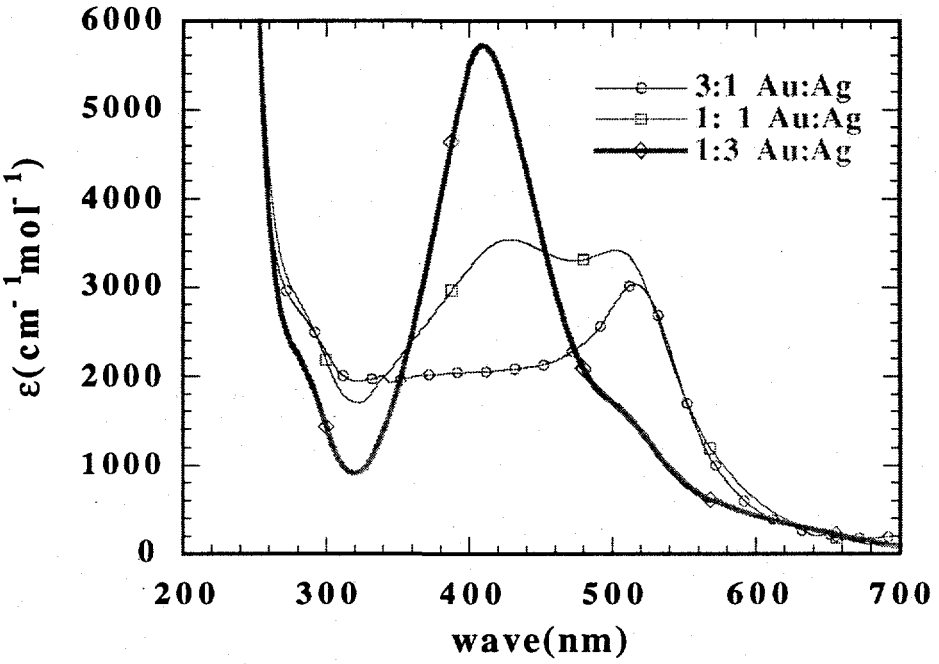

Figure 34. Effect of composition on the optical absorbance of 10 nm Au:Ag composite clusters with a gold core and a silver coating. As expected, the optical features begin to resemble those of the main component as the other component concentration decreases. The molar ratio of Au:Ag is indicated in the figure.

VII. Future Research Directions

In this work we have produced many unique nanocluster materials and have made considerable progress toward understanding their optical, magnetic and dielectric properties. We have greatly improved the micellar synthesis process and in the latter phases of the program established a capability for the purification of nanoclusters using high performance liquid chromatography. This processing technique includes on-line optical diagnostic measurements such as absorbance, conductivity and photoluminesence. This development represents a signficiant advance in the field of nanoclusters and has enabled measurements of nanocluster properties which have previously escaped detection.

Due to this research, many interesting new properties of these materials have been revealed for the first time, and we anticipate and urge active research within Sandia and elsewhere on practical catalytic reactions using these new materials. Indeed this is an important aspect of our recently-funded BES initiative on the synthesis and processing of nanoclusters for energy applications which was an outgrowth of this LDRD program. and of the BES Center for Synthesis and Processing project on nanoscale materials. We also expect these materials will prove very useful because of their inertness, lack of toxicity, and low cost (particularly Fe and FeS_2) and will serve as an entirely new class of photooxidation catalysts for the destruction of organic wastes using sunlight (solar detoxification). We also urge further work on processing these new materials into forms suitable for the intended applications.

Acknowledgments

The authors would like recognize the valuable assistance of Sharon Craft in the synthesis of the materials used in this LDRD project and of Leonard Hensen in performing the measurements of dielectric properties.

References

[1] "Research Opportunities on Clusters and Cluster-Assembled Materials - A Department of Energy, Council on Materials Science Panel Report, J. Mater. Res., 4(3), 704-736, (1989).

[2] J.P. Wilcoxon, A. Martino, A..P. Sylwester, R. Williamson, and R. Baughman, "Novel Catlysts Based on Microemulsions", SAND report, Sandia National Laboratories, Albuquerque, N.M., Oct. 1992.

[3] Wilcoxon, J.P., DOE patent #5,147,841, DOE control #S 70621, entitled "Method for the Preparation of Metal Colloids in Inverse Micelles and Product preferred by the method", issued Sep. 15, 1992.

[4] A. Martino, J.P. Wilcoxon, and J. Kawola , "Synthesis and Characterization of Fe and FeS_2 (Pyrite) Coal Liquefaction Catalysts in Inverse Micelles", Energy and Fuels, xx, xx, (1994)."

[5] Wilcoxon J.P., Martino T., E. Klavetter, and Sylwester A.P., "Synthesis and Catalytic Properties of Metal and Semiconductor Nanoclusters", in Nanophase Materials, proceedings of the NATO ASI, Corfu, Greece, June 1993.

[6] See A. D. Yoffe, Adv. in Phys. **42**, 173 (1993) for a recent review and references therein.

[7] R. F. Frindt and A. D. Yoffe, Proc. Roy. Soc. A., **273**, 69 (1963).

[8] B. L. Evans and P. A. Young, Proc. Roy. Soc. A., **284**, 402 (1965).

[9] R. Coehoorn, C. Haas, J. Dijkstra, C.J.F. Flipse, R.A. deGroot and A. Wold, Phys. Rev. B., 35, 6195 (1987), **35**, 6203 (1987).

[10] Al. L. Efros and A.L. Efros, Sov. Phys. Semicond. **16**, 772 (1982).

[11] L.E. Brus, IEEE J. Quant. Electron **QE-22**, 1909 (1986).

[12] Y. Kayanuma, Phys. Rev. B. **38**, 9797 (1988), 44,13085 (1991).

[13] J.P. Wilcoxon and G.A. Samara, "Strong Quantum-Size Effects in a Layered Semiconductor: MoS2 Nanoclusters", Phys Rev. B 51, 7299, (1995).

[14] J.P. Wilcoxon and G.A. Samara, "Strong Quantum Confinement Effects in Semiconductors: FeS_2 Nanoclusters", Appl Phys Lett, in prep.

[15] I.S. Jacobs and C.P. Bean in Magnetism, edited by G. T. Rado and H. Suhl (Academic Press, New York, 1963), Vol. III, pp. 271-350, and references therein.

[16] W.F. Brown, Jr., Micromagnetics (Wiley Interscience, New York, 1963.

[17] E.P. Wohlfarth in Magnetism, edited by G. T. Rado and H. Suhl (Academic Press, New York, 1963), Vol. III, pp. 351-393.

[18] E. Kneller in Magnetism and Metallurgy, edited by A. Berkowitz and E. Kneller (Academic Press, New York, 1969), Vol. 1, pp. 365-471 and references therein.
[19] S. Gangopadhyay, G.C. Hadjipanayis, S.I. Shah, C.M. Sorensen, K.J. Kablunde, V. Papaefthymiou, A. Kostikas, J. Appl. Phys. 70, 5888 (1991).
[20] S. Gangopadhyay, G.C. Hadjipanayis, B. Dale, C.M. Sorensen, K.J. Kablunde, V. Papaefthymiou, A. Kostikas, Phys. Rev. B 45, 9778 (1992).
[21] A. Tsoukatos, H. Wan, G.C. Hadjipanayis, V. Papaefthymiou, A. Kostikas, A. Simopoulos, J. Appl. Phys. 73, 6967 (1993).
[22] A. Tasaki, S. Tomiyama, S. Iida, N. Wada, R. Uyeda, Jpn. J. Appl. Phys. 4, 707 (1965).
[23] J.P. Wilcoxon, R.L. Williamson, R.J. Baughman, J. Chem. Phys. 98, 9933 (1993).
[24] B. M. Berkovsky, V. F. Medvedev, M.S. Krakov, Magnetic Fluids: Engineering Applications (Oxford Univ. Press, Oxford, 1993), p. 12.
[25] L. Neel, Compt. Rend. 228, 664 (1949).
[26] C.P. Bean and J.D. Livingston, J. Appl. Phys. 30 (supplement), 120S (1959).
[27] For example, W.F. Brown, Jr., J. Appl. Phys. 30 (supplement), 130S (1959).
[28] I.M. Billas, J.A. Becker, A. Chatelain, W.A. de Heer, Phys. Rev. Lett. 71, 4067 (1993).
[29] F.E. Luborsky, J. Appl. Phys. 32 (supplement), 171S (1961) and references therein.
[30] E. L. Venturini, J. P. Wilcoxon and P. P. Newcomer, "Magnetic Properties of Nanosize Iron Clusters", proceedings of the spring MRS, San Francisco, CA, Apr 1994,.
[31] L.P. Gor'kov and G. M Eliashberg, Sov. Phys. - JETP 21, 940 (1965).
[32] W. P. Halperin, Rev. Mod. Phys. 58, 533 (1986).
[33] G. Nimtz and P. Marquardt, Phil. Mag. Letters 61, 231 (1990) and references therein. See also Phys. Rev. B __, (199?).
[34] Wilcoxon J., Sylwester A., Nigrey P., Martino A., Quintana C., and Baughman R., "Formation and Characterization of Highly-Dispersed Iron Catalysts", in the Eighth Annual International Pittsburgh Coal Conference Proceedings, 703-708, (1991).
[35] J. A. A. J. Perenboom, P. Wyder and F. Meier, Phys. Reports 78, 173 (1981).
[36] P. V. Ashrit, G. Bader, S. Badilescu, F. E. Girouard, L. Nguyen and V. Truong, J. Appl. Phys. 74, 602 (1993).
[37] S. P. Appell, J. Giraldo and S. Lundquist, Phase Transitions 24-26, 577 (1990).
[38] M. Faraday , Transactions of the Faraday Society, 145 ,(1857).
[39] S. Tadao, Advances in Colloid and Interface Science, **28**, 16, (1987).
[40] A. Henglein, Chem. Rev., **89**, 1861, (1989).
[41] U. Kreibig, and L. Genzel, Surf. Sci., **156**, 678, (1985).

[42] S.M. Heard, F. Grieser, and C.G. Barraclough, J. Coll. Inter. Sci., **93**, 545, (1983).

[43] D. R. Huffman in *Optical Properies Associated with Small Particles,* ed. R.K. Chang and P.N. Barber, World Scientific, 1990.

[44] J. Hillier, J. Turkevich, and P.C. Stevenson, Trans. Faraday Soc. Discussion **11**, 55, (1951).

[45] J. Turkevich, G. Garton, and P.C. Stevenson, J. Colloid Sci., Suppli. #1, 26, (1954).

[46] *Optical Constants of Solids*, Ed D. Palik, Academic Press, (1985).

[47] D. Schonauer, H. Lauer, and U. Kreibig, Z. Phys. D, **20**, 301, (1991).

[48] CRC Handbook of Chemistry and Physics, 66th Ed.

[49] M. Kerker, "The Optics of Colloidal Silver: Something Old and Something New", J. Coll. and Inter. Sci., 105,(2), 297, (1985).

Appendix

List of publications and Presentations

Publications

J.P. Wilcoxon, G. Samara, and P. Newcomer, **Optical Features of Nanosize Iron and Molybdenum Sulfide Clusters**, Proceedings of Symposium F, meeting of the MRS Society, Boston, MA., (1995).

J.P. Wilcoxon and G.A. Samara, **Strong Quantum-Size Effects in a Layered Semiconductor: MoS_2 Nanoclusters**, Physical Rev B 51, 7299 (1995).

Venturini E.L., Wilcoxon J.P., and Newcomer P.P., **Magnetic Properties of Nanosize Iron Clusters**, Symposium V, Proceedings of the Spring Meeting of the Materials Research Soc., San Francisco, CA. (1994).

A. Martino, J.P. Wilcoxon, and J. Kawola , **"Synthesis and Characterization of Fe and FeS_2 (Pyrite) Coal Liquefaction Catalysts in Inverse Micelles"**, Energy and Fuels, 8, 1289 (1994).

Wilcoxon J.P., Martino T., E. Klavetter, and Sylwester A.P., **Synthesis and Catalytic Properties of Metal and Semiconductor Nanoclusters**, in Nanophase Materials, ed. G. Hadjipanaysis and D. Siegel, Kluwer Acad. Pub., 770-780, 1994.

Presentations:

.P. Wilcoxon, G. Samara, and P. Newcomer, **Optical Features of Nanosize Iron and Molybdenum Sulfide Clusters**, Symposium F, 1994 meeting of the MRS Society, Boston, MA.

J.P. Wilcoxon, G. Samara, and P. Newcommer, **Optical and Catalytic Properties of Nanosize Metal Sulfide Clusters**, 1994 meeting of the American Physical Society, March 22 1994, Pittsburgh, PA

Venturini E.L., Wilcoxon J.P., and Newcomer P.P., **Magnetic Properties of Nanosize Iron Clusters**, Symposium V, Spring Meeting of the Materials Research Soc., San Francisco, CA. (1994).

E.L Venturini, J.P. Wilcoxon, P.P. Newcomer, and G.A. Samara, **Static Magnetic Properties of Nanosize Iron Clusters**, 1994 meeting of the American Physical Society, March 22 1994, Pittsburgh, PA

Wilcoxon J.P., Martino T., E. Klavetter, and Sylwester A.P., **Synthesis and Catalytic Properties of Metal and Semiconductor Nanoclusters**, in Nanophase Materials, NATO ASI meeting, Corfu, Greece, June 1993. (invited)

J.P. Wilcoxon, G. Samara, and P. Newcomer, **Strong Quantum-Size Effects in a Layered Semiconductor: MoS_2 Nanoclusters**, 1993 meeting of the American Physical Society, March 22, 1993, Seattle, WA.

J. Wilcoxon, G. Samara, A. Martino, and R. Baughman, **Synthesis and Size-Dependent Optical, Dielectric, and Catalytic Properties of Metal Clusters,** 1993 meeting of the American Physical Society, March 22, 1993, Seattle, WA.

A. Martino, J. Wilcoxon, A.P. Sylwester, and J.S. Kawola, **Synthesis and Characterization of Fe and FeS2 (pyrite) Catalysts Particles in Inverse Micelles,** Proceedings of the 205th National American Chemical Soc. meeting, Miami, (1993).

List of Invention Disclosures:

None

List of patents:

None

List of copyrights:

None

Employee recruitment

D. E. Bliss hired as Post Doc

Student Involvement:

None

Follow On Work:

New BES initiative on Nanoclusters for Energy Applcations funded.

Distribution:

1	MS-1436	C. E. Meyers, 1007
1	MS-1427	P. L. Mattern, 1100
1	MS-1421	P. P. Newcomer, 1152
10	MS-1421	G. A. Samara, 1152
5	MS-1421	J. P. Wilcoxon, 1152
1	MS-1421	E. B. Stechel, 1153
1	MS-1421	E. L. Venturini, 1153
1	MS-1134	B. K. Damkroger, 1833
1	MS-1134	R. L. Williamson, 1833
1	MS-9018	Central Tech Files, 8523-2
5	MS-0899	Technical Library, 13414
1	MS-0619	Print Media, 12615
2	MS-0100	Document Processing, 7613-2
44		DOE/OSTI